An Examination of Soil Crusts on the Floor of Jezero Crater, Mars

E. Hausrath, C. Adcock, A. Bechtold, P. Beck, K. Benison, A. Brown, E. Cardarelli, N. Carman, B. Chide, J. Christian, et al.

JGR Planets

RESEARCH ARTICLE
10.1029/2022JE007433

Special Section:
The Mars Perseverance Rover Jezero Crater Floor Campaign

An Examination of Soil Crusts on the Floor of Jezero Crater, Mars

E. M. Hausrath[1], C. T. Adcock[1], A. Bechtold[2], P. Beck[3], K. Benison[4], A. Brown[5], E. L. Cardarelli[6], N. A. Carman[1], B. Chide[7], J. Christian[8], B. C. Clark[9], E. Cloutis[10], A. Cousin[11], O. Forni[11], T. S. J. Gabriel[12], O. Gasnault[11], M. Golombek[6], F. Gómez[13], M. H. Hecht[14], T. L. J. Henley[15], J. Huidobro[16], J. Johnson[17], M. W. M. Jones[18], P. Kelemen[19], A. Knight[8], J. A. Lasue[11], S. Le Mouélic[20], J. M. Madariaga[16], J. Maki[6], L. Mandon[21], G. Martinez[22], J. Martínez-Frías[23], T. H. McConnochie[9], P.-Y. Meslin[11], M.-P. Zorzano[13], H. Newsom[24], G. Paar[25], N. Randazzo[26], C. Royer[27], S. Siljeström[28], M. E. Schmidt[15], S. Schröder[29], M. A. Sephton[30], R. Sullivan[31], N. Turenne[10], A. Udry[1], S. VanBommel[8], A. Vaughan[32], R. C. Wiens[33], N. Williams[6], and the SuperCam team and the Regolith working group[34]

[1]Department of Geoscience, University of Nevada, Las Vegas, NV, USA, [2]Department of Lithospheric Research, University of Vienna, Vienna, Austria, [3]University of Grenoble Alpes, CNRS, IPAG, Grenoble, France, [4]Department of Geology and Geography, West Virginia University, Morgantown, WV, USA, [5]Plancius Research, Severna Park, MD, USA, [6]Jet Propulsion Laboratory, California Institute of Technology, Pasadena, CA, USA, [7]Los Alamos National Laboratory, Los Alamos, NM, USA, [8]Department of Earth and Planetary Sciences, Washington University in St. Louis, St. Louis, MO, USA, [9]Space Science Institute, Boulder, CO, USA, [10]Department of Geography, University of Winnipeg, Winnipeg, MB, Canada, [11]Institut de Recherche en Astrophysique et Planétologie, Université de Toulouse 3 Paul Sabatier, CNRS, CNES, Toulouse, France, [12]US Geological Survey, Flagstaff, AZ, USA, [13]Centro de Astrobiologia (CSIC-INTA), Madrid, Spain, [14]Haystack Observatory, Massachusetts Institute of Technology, Westford, MA, USA, [15]Department of Earth Science, Brock University, St. Catharines, ON, Canada, [16]Department of Analytical Chemistry, University of the Basque Country UPV/EHU, Leioa, Spain, [17]John Hopkins University Applied Physics Laboratory, Laurel, MD, USA, [18]Central Analytical Research Facility and School of Chemistry and Physics, Queensland University of Technology, Brisbane, QLD, Australia, [19]Columbia University, New York City, NY, USA, [20]Laboratoire de Planétologie et Géosciences, CNRS, UMR 6112, Nantes Université, University Angers, Nantes, France, [21]LESIA, Observatoire de Paris, Université PSL, CNRS, Sorbonne Université, Université de Paris, Meudon, France, [22]Lunar and Planetary Institute, Houston, TX, USA, [23]Instituto de Geociencias, Madrid, Spain, [24]University of New Mexico, Albuquerque, NM, USA, [25]Joanneum Research, Graz, Austria, [26]Department of Earth and Atmospheric Sciences, University of Alberta, Edmonton, AB, Canada, [27]Observatoire de Paris, LESIA, CNRS, Université PSL, Sorbonne Université, Université de Paris, Meudon, France, [28]RISE Research Institutes of Sweden, Stockholm, Sweden, [29]Deutsches Zentrum für Luft- und Raumfahrt (DLR), Institute of Optical Sensor Systems (OS), Berlin, Germany, [30]Department of Earth Science & Engineering, Imperial College, London, UK, [31]CCAPS, Cornell University, Ithaca, NY, USA, [32]Apogee Engineering, LLC, Flagstaff, AZ, USA, [33]Earth, Atmospheric and Planetary Sciences, Purdue University, West Lafayette, IN, USA, [34]See Table S4 and S5

Key Points:

- Soil crusts are prevalent across the Jezero crater floor
- Soil surfaces are largely hydrated
- Soil crusts likely contain salts and may form during changes in atmospheric relative humidity at the surface

Supporting Information:

Supporting Information may be found in the online version of this article.

Correspondence to:

E. M. Hausrath,
Elisabeth.Hausrath@unlv.edu

Citation:

Hausrath, E. M., Adcock, C. T., Bechtold, A., Beck, P., Benison, K., Brown, A., et al. (2023). An examination of soil crusts on the floor of Jezero crater, Mars. *Journal of Geophysical Research: Planets*, *128*, e2022JE007433. https://doi.org/10.1029/2022JE007433

Received 29 JUN 2022
Accepted 4 JAN 2023

Abstract Martian soils are critically important for understanding the history of Mars, past potentially habitable environments, returned samples, and future human exploration. This study examines soil crusts on the floor of Jezero crater encountered during initial phases of the Mars 2020 mission. Soil surface crusts have been observed on Mars at other locations, starting with the two Viking Lander missions. Rover observations show that soil crusts are also common across the floor of Jezero crater, revealed in 45 of 101 locations where rover wheels disturbed the soil surface, two out of seven helicopter flights that crossed the wheel tracks, and four of eight abrasion/drilling sites. Most soils measured by the SuperCam laser-induced breakdown spectroscopy (LIBS) instrument show high hydrogen content at the surface, and fine-grained soils also show a visible/near infrared (VISIR) 1.9 μm H_2O absorption feature. The Planetary Instrument for X-ray Lithochemistry (PIXL) and SuperCam observations suggest the presence of salts at the surface of rocks and soils. The correlation of S and Cl contents with H contents in SuperCam LIBS measurements suggests that the salts present are likely hydrated. On the "Naltsos" target, magnesium and sulfur are correlated in PIXL measurements, and Mg is tightly correlated with H at the SuperCam points, suggesting hydrated Mg-sulfates. Mars Environmental Dynamics Analyzer (MEDA) observations indicate possible frost events and potential changes in the hydration of Mg-sulfate salts. Jezero crater soil crusts may therefore form by salts that are hydrated by changes in relative humidity and frost events, cementing the soil surface together.

Plain Language Summary Martian soils are important for understanding the history of Mars as well as future sample return and human exploration. Soil crusts in Jezero crater, which are also broadly found across Mars, can be observed when they are disturbed, such as by rover wheels or coring/abrasion activities. Jezero crater soil crusts are examined using images from the Perseverance and Ingenuity cameras, as well as using data from the SuperCam, PIXL, Mastcam-Z, and MEDA instruments. Soil crusts are common in Jezero crater and show characteristics including hydration at the surface and the presence of salts that might contain water. MEDA instrument measurements indicate that changes in the hydration state of salts may result during conditions measured at Jezero crater. Jezero crater soil crusts may therefore form by salts that are present on the surface that can add or lose water during changes in relative atmospheric humidity and frost events. These changes in the amount of water present in the salts may result in soil surfaces that are cemented together, forming the crusts observed at Jezero crater. A better understanding of Mars soil crusts will help in the understanding of samples returned to Earth from Mars, as well as future human exploration.

1. Introduction

Much of the surface of Mars is covered by soils. These soils allow an investigation of the integrated history of the surface, including different geological, hydrological, atmospheric, and if life were present, microbiological processes. Understanding soils is important to the four goals of the Mars 2020 *Perseverance* mission, which are to (a) determine whether life ever existed on Mars, (b) characterize the climate of Mars, (c) characterize its geology, and (d) prepare for human exploration (Mustard et al., 2013). A comprehensive understanding of soils is also valuable to the success of the Mars Sample Return Program, as outlined in the iMOST report (iMOST, 2018), as Martian soils are outstanding heterogeneous samples that will yield large amounts of information relevant both to science and future human exploration after their return to Earth and detailed characterization.

Soil crusts represent increased cohesion at the surface compared with deeper materials. Soil crusts have been observed on Mars at other lander and rover sites, including Viking Lander 1 (Clark et al., 1982), Mars Pathfinder (Brückner et al., 2003), along both Mars Exploration Rover traverses (Arvidson et al., 2010) and along the Mars Science Laboratory (MSL) traverse (Blake et al., 2013). On Earth, salts can form cohesive crusts and provide habitable environments (e.g., Hughes & Lawley, 2003; Marchant & Head, 2007; Wierzchos et al., 2011). On Mars, soil crusts can also protect subsurface minerals from direct exposure to Martian surface conditions, allowing otherwise unstable minerals to persist at depth (Wang et al., 2008). An understanding of these crusts and their origins may therefore shed light on potentially habitable surface or near-subsurface environments in the Martian past. In addition to thin surface crusts, Martian soil is weakly cohesive to depths of 10 cm or more, as revealed in standing trench walls created by the Viking Lander sampling arm (Moore et al., 1987) and rover wheel trenches (e.g., Sullivan et al., 2011). Understanding soil crusts and subsurface cohesion by in situ measurements on Mars is also critical to understanding returned soil samples as the spatial distribution in returned samples will not be preserved within the sample tube after sampling (Moeller et al., 2021). Despite the prevalence and importance of Martian surface crusts, their characteristics and formative mechanisms remain poorly understood.

The soil crusts at the Viking 1 landing site (Clark et al., 1982) and detected by the Sojourner rover were rich in sulfate and chlorine (Brückner et al., 2003). The soil crusts analyzed by Spirit were rich in iron-sulfate and chlorine salts (Arvidson et al., 2010), while the crusts analyzed by Opportunity were enriched in magnesium-sulfate, with other metal-sulfates present to a lesser extent (Arvidson et al., 2011). Salts containing metal-chlorine compounds were also analyzed by Opportunity (Arvidson et al., 2011). The analysis of water-soluble salts in soils performed by the wet chemistry laboratory of the Phoenix lander showed around 1.1% sulfate compounds in the soil (Kounaves et al., 2010), consistent with a major magnesium-sulfate mineral (epsomite was suggested) and a minor calcium-sulfate mineral (gypsum was suggested). Analysis by the Phoenix wet chemistry laboratory also showed an equivalent amount of 0.4%–0.6% ClO_4^-, potentially as $Mg(ClO_4)_2$ (Hecht et al., 2009) and $Ca(ClO_4)_2$ (Kounaves et al., 2014), and likely also containing ClO_3^- (Hanley et al., 2012). Sulfate crusts on Mars have been proposed as resulting from the alteration of in situ sulfides and pyroxenes by melt water leading to their formation (Fishbaugh et al., 2007). These observations from multiple landing sites on Mars indicate the importance of salts in Martian soil crusts.

On Earth, salt crusts can form by the efflorescent growth of mineral crystals that precipitate when saline groundwaters are wicked to the subaerial surface by high rates of evaporation, forming mm-scale or smaller crystals of salt minerals (Smoot & Castens-Seidell, 1994). The tiny crystals can form a mm-to-cm-scale stratum at the surface on top of unconsolidated sediments or directly on rocks, or they can form an intergranular cement that

weakly lithifies the topmost part of a sediment. Efflorescent crusts tend to have a bumpy surface that effectively traps windblown sediments (Benison, 2019; Benison et al., 2007). Such efflorescent salt crusts can be eroded by wind and redeposited, contributing to cemented surface accumulations of crystals found in some arid terrestrial environments (Benison, 2017). Several studies of sulfate-rich minerals have detected amino acids (Aubrey et al., 2006; Skelley et al., 2005) and lipids (Tan et al., 2018), revealing the utility of these salt-rich deposits for capturing and preserving molecular markers of past life. Additionally, the SHERLOC instrument on *Perseverance* has recently shown colocalization of sulfates and aromatic molecules in rocks from the Séítah and Máaz formations, suggesting the preservation of organic molecules by sulfates on Mars (Scheller et al., 2022; Sharma et al., 2022). Sulfate minerals have also been shown to be effective at trapping whole organisms within crystals (Edwards et al., 2005), with salt crusts able to both protect surficial microorganisms from the surface environment and impede their detection (Cloutis et al., 2021). Past salt crusts on Mars, however, would have been subject to potentially harsh surface conditions.

The atmospheric origin of salt crusts on soil surfaces is also increasingly recognized as important in hyperarid regions on Earth. The gas phase oxidation of chlorine-compounds to perchlorate can explain observations in both the Atacama Desert and on Mars (Catling et al., 2010) with yields being assisted by silica and metal oxides acting as photocatalysts (Carrier & Kounaves, 2015). Nitrate and sulfate salts can also be delivered by atmospheric mechanisms in hyperarid regions on Earth (Ericksen, 1981), a hypothesis at least partly supported by isotopic measurements of Atacama nitrate (Michalski et al., 2003) and sulfate (Bao et al., 2004). Similar processes may have operated on Mars. Nitrate, perchlorate, and iodate have been shown to cooccur in terrestrial deserts (Lybrand et al., 2016), and nitrates have been detected in regolith on Mars in concentrations up to hundreds of ppm (Stern et al., 2015). Salt crusts are also present in Antarctica, where they can serve as habitats for microorganisms (Hughes & Lawley, 2003; Marchant & Head, 2007). Because the top most layer of the Martian soil is in contact with the Martian atmosphere, if atmospheric humidity is sufficiently high, hygroscopic salts such as perchlorates, sulfates, and chlorides can absorb moisture from the air, changing the hydration state and deliquescing and forming brines that have been shown to form crusts in Mars analog regolith in laboratory experiments (Ramachandran et al., 2021).

This paper reports morphologic and compositional characteristics of soil crusts encountered on the floor of Jezero crater up to sol (Martian day) 378 of the Mars 2020 (M2020) mission. This corresponds to Martian solar longitudes (L_s) 10–190°. Rover images from the Navcam and Hazcam engineering cameras (Maki et al., 2020a, 2020b), the higher resolution multispectral Mastcam-Z system (Bell & Maki, 2021; Hayes et al., 2021), and helicopter images enabled identification of soil crusts exposed in the wheel and abrasion/drilling disturbances along the rover traverse. Crust compositions were measured using the mast-mounted SuperCam (Maurice et al., 2021; Wiens, Maurice, Robinson, et al., 2021), and arm-mounted Planetary Instrument for X-ray Lithochemistry (PIXL; Allwood et al., 2020) instruments. Environmental conditions affecting soil surfaces were also evaluated, using the rover's Mars Environmental Dynamics Analyzer (MEDA) suite of environmental sensors (Rodriguez-Manfredi et al., 2021). Together, these measurements help to understand soil crusts in Jezero crater, their formation mechanisms, and their importance to both sample return and human exploration.

2. Materials and Methods

2.1. Identification of Soil Crusts in Images

To examine the prevalence of soil crusts at Jezero crater, Rear Hazcam red-green-blue (RGB) color images were examined at each rover stop through sol 378 for evidence of soil crusts. Where Rear Hazcam images did not show evidence of surface crust, Navcam RGB color images were also examined. When Rear Hazcam images were not obtained, Front Hazcam images were examined. Many of these images allowed examination of locations where surface soil was disturbed by rover wheels, potentially displaying evidence of surface crust through surface fracturing and/or minor "rafting" lateral displacements (Figure S1 in Supporting Information S1). Images that did not show evidence of surface crust do not necessarily indicate that a crust was not present; wheel pressure causing pure vertical displacement of surface material only to very shallow depths, with no lateral displacement of materials, is unlikely to reveal the presence of surface crust (i.e., the presence of a thin surface layer with slightly more cohesion than underlying soil). Where helicopter flights crossed the tracks, the helicopter images were examined to detect the presence of fractures or "rafting" consistent with surface crust. Images near each coring and abrasion site were also examined to identify evidence of crusts disturbed by the coring and abrasion activities. To understand the characteristics of the surface that formed the crust, the grain size distribution of the surfaces that contained crusts was also examined consistent with other work (Cousin et al., 2015; Vaughan et al., 2023).

2.2. Quantification of Soil Crusts Using Stereo Imaging

Three-dimensional analysis of the soil disturbed by the wheel tracks and by the coring and abrasion activities was performed using stereo color images obtained from the Mastcam-Z (Bell & Maki, 2021; Hayes et al., 2021; Kinch et al., 2020), including steep microslopes formed by rocks that were pushed into the soil by the rover wheels, sidewalls of cracks caused by soil disturbance, and rigid clods of compacted soil released by the wheels and moved along the surface (Figure 1). Surfaces disturbed by the coring/abrasion activities allowed the quantification of the thickness of the crust. Images were also examined for slopes that are greater than the angle of repose for sands on Mars, which according to Atwood-Stone and McEwen (2013) is between 30° and 34°. The characteristics of the wheel tracks, (i.e., their depth and shape), were also examined as indicators of soil cohesion. These phenomena were quantified using 3D data analysis (Paar et al., 2023) (Figure 1, Table S2).

2.3. Examination of the Surface Using the PIXL Instrument

Naltsos was the first rock analyzed by PIXL, consisting of a 120-spot line scan with ∼120 μm interrogation spots (Allwood et al., 2020) and an intended spacing of ∼250 μm. The Naltsos rock is a low-standing, relatively flat "paver" rock attributed to the Máaz formation (Sun et al., 2023), chosen as a target primarily due to its suitability for several engineering first time activities, including PIXL placement. To help understand the soil crust, PIXL data from the soil, dust, and dust-crust-covered rock Naltsos are also compared to the soil crust to allow assessment of the processes impacting soil crust formation.

2.4. Examination of Soil Surfaces Using SuperCam

2.4.1. Remote Microimager (RMI)

All of the SuperCam laser-induced breakdown spectroscopy (LIBS) measurements of soils through sol 378 were analyzed for this study, including LIBS observations of rocks with soils on top of them, using the SuperCam instrument on the Mars2020 *Perseverance* rover (Maurice et al., 2021; Wiens, Maurice, Robinson, et al., 2021). SuperCam's RMI (Gasnault et al., 2021; Maurice et al., 2021) provides pictures for local context and site imaging at a high-resolution for each of these LIBS measurements. The 110-mm SuperCam telescope with a focal length of 563 mm allows it to take RGB color images of 2,048 × 2,048 pixels with a CMOS camera over a bandwidth from ∼375 to ∼655 nm (Maurice et al., 2021; Wiens, Maurice, Robinson, et al., 2021). It is useful to preselect and visualize grains, textures, color differences, and other features of the potential soil targets (contextualizing them in their respective geomorphological settings), which can help interpret further chemical analyses. RMI data are available on the Planetary Data System (Wiens, Maurice, Deen, et al., 2021).

2.4.2. Laser Induced Breakdown Spectroscopy (LIBS)

LIBS measurements provide major and trace element detection and quantification (Maurice et al., 2021; Wiens, Maurice, Robinson, et al., 2021). LIBS measurements are usually performed as rasters of 5–10 "points" on each target using a focused laser beam 250–350 μm in diameter. At each point, 30–50 laser pulses ("shots") were used. Individual ("single-shot") spectra can be analyzed, or all spectra for that point can be averaged for better statistics. LIBS data are available on the Planetary Data System (Wiens, Maurice, Deen, et al., 2021) and the points used in this paper are listed in Table 1.

The LIBS measurements of the soils were analyzed in the following ways: (a) the hydrogen score (Forni et al., 2013), as a function of shot, was examined to analyze differences with depth; (b) the standard deviation of the total LIBS emissivity was examined to identify fine-grained particles versus coarse grains after Cousin et al. (2015); (c) the average LIBS Major-element Oxide Composition (MOC) data and the H, Cl, and S scores were examined using principal component analysis (PCA) to examine different elemental correlations; (d) the shot-to-shot data for Naltsos were examined using PCA for comparison with the PIXL data; and (e) the SuperCam LIBS Major-element Oxide Composition data and H, Cl, and S scores of the disturbed soils were averaged and compared to the fine soils that are high in H. Each analysis is further described below.

Repeated laser pulses at each observation point form small excavation pits in soils, allowing chemical variations in the top 1–2 mm (Meslin et al., 2013) to be examined. To examine whether the soil crust is potentially hydrated, the hydrogen independent component analysis (ICA) score was compared as a function of shot number as a proxy for depth. The hydrogen score is a unitless measure of the hydrogen peak that can correspond to the hydrogen

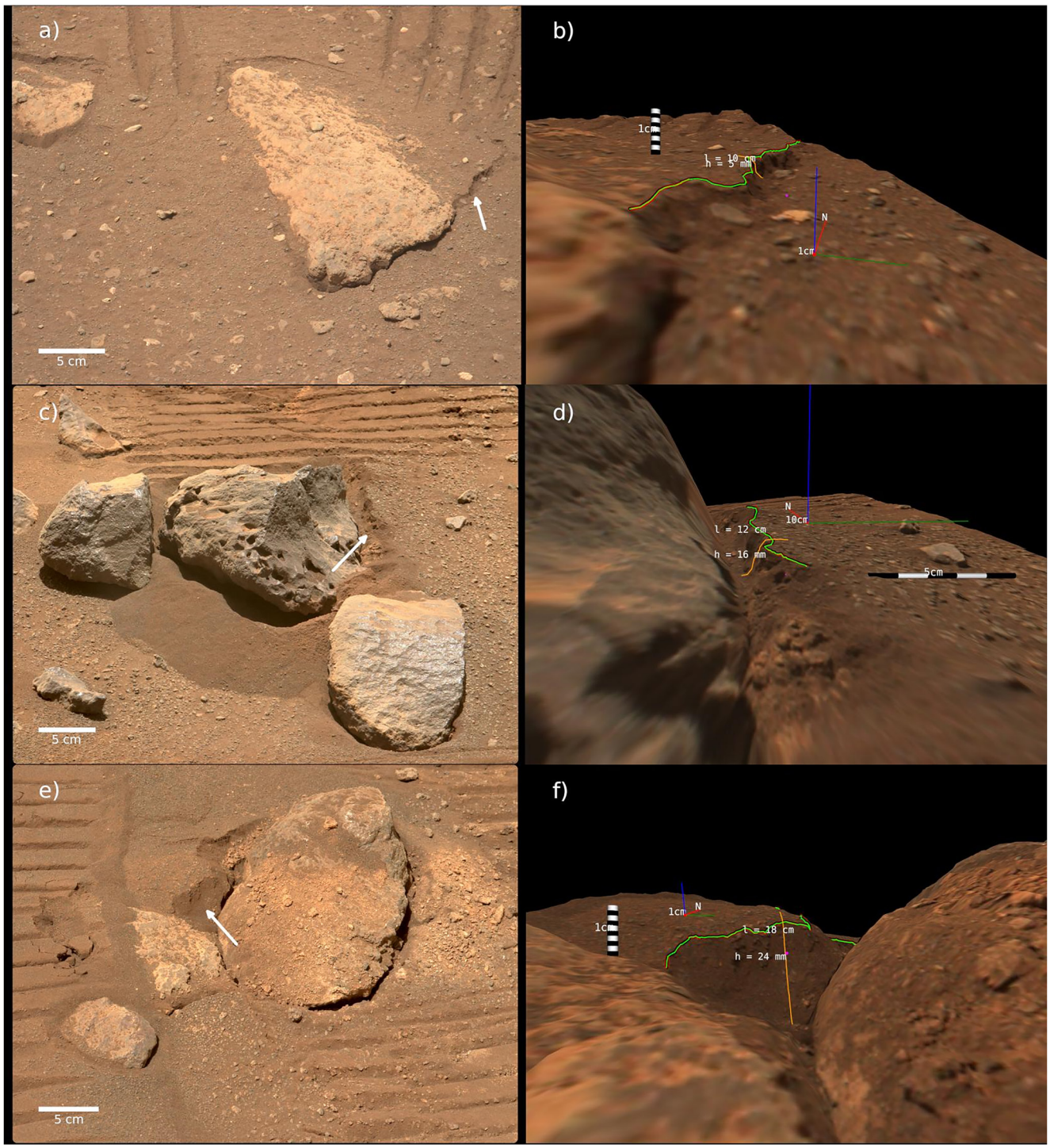

Figure 1. Radiometrically calibrated Mastcam-Z images (left) and derived 3D visualization products (right) showing regions indicating soil crusts and their morphological parameters observed by Perseverance in Jezero crater, Mars. These soil crust candidate regions are indicated by physical disturbances on or close to the rover tracks. In some cases, they are directly visible from edges (see white arrows) that formed when small rocks were moved by the rover wheels. (a) Image from sol 15 showing several soil crust edges. (b) 3D product derived from (a) showing a measured height of 5 mm (angle = 53°). (c) Image from sol 150 showing a soil crust edge next to a rock and rover tracks in the upper part. (d) 3D product derived from (c) showing a measured height of 16 mm (angle = 57°). (e) Image from sol 335 showing a soil crust edge. (f) 3D product derived from (e) showing a height of 24 mm (angle = 40°). Ordered Point Clouds (OPCs), visualized by PRo3D as shown in this figure, are available under ftp://PRoViP-Mastcam-Z-PDS-Released@dig-sftp.joanneum.at:2200/ with user name "PRoViP-Mastcam-Z-PDS-Released" and password "MQRr63hJdUzVFHYc!". PRo3D, the Planetary Robotics 3D Viewer, can be accessed via https://github.com/pro3d-space/PRo3D The Mastcam-Z data are available in the Planetary Data Service (PDS) (Bell & Maki, 2021). The Sequence ID numbers are Sol 15: zcam08000, Sol 150: zcam03189, Sol 335: zcam03305. Image credit: NASA/JPL-Caltech/ASU/MSSS.

Table 1
Laser-Induced Breakdown Spectroscopy (LIBS) Data Used Through Sol 378

Target	Sol	Points	Comments
Daa	357	1, 4–10	2 and 3 are on a rock
Toudon	333	1–9	4–9 = disturbed
Sigonce	319	1–10	
Chandon	315	1, 5, 10	Only 1, 5, 10 in focus; 10 = disturbed
Tanaron	313	1, 5, 10	Only 1, 5, 10 in focus
Brandis	302		All points (1–10) disturbed—not used in this work due to apparent rock surface
Rougon	282	1–10	4–10 = disturbed
Courbaissa	238	2–3	Points 2–3 in soil on a rock
Vaire	236	1–10	
Vaire	214	1–10	
Chambares	185	1–10	
Reglet	151	8–10	Soil at the edge of a paver
Clave	150	1–10	
Croix	145	1–10	
Beujeau	140	6	Soil on a rock
Roque	137	1	Soil next to a rock
Whoosh	123	1–10	
Cheskeh	116	1–10	
Que_eh_SCAM	115	1–10	
Lha_tsaadah	110	1–10	
Hastaa	106	1–10	
Asdzoh	103	1–4	Soil at the edge of a rock
Sei	84	1–5	
Naakih	84	1–5	
A_koo	72	1–10	
Naltsos	126	1–5	On dusty rock for comparison with PIXL analyses

content, and the hydrogen score is obtained using an ICA analysis described by Forni et al. (2013). It was also used by Meslin et al. (2013) for their analysis of the ChemCam soil observations. The retrieved H component, which is used to compute the hydrogen score, and is specific to the SuperCam instrument, is displayed in Figure S7 of Supporting Information S1 and reported in Table S1. The average hydrogen ICA score of points 6–10 (removing the top five points to remove the effect of loose dust) was compared with the average of the deepest 10 shots of each sample to determine whether a statistically significant decrease in H from the surface was observed; the averages of scores 6–10 were also compared to determine whether different points were above or below the average.

For comparison with the RMI images of the soils, we also measured the standard deviation of the total emissivity of the LIBS measurements for shots >10. The standard deviation of the total emissivity of the LIBS measurement has been previously shown to indicate the presence of a coarse grain versus fine grains (Cousin et al., 2015). Measurements of the standard deviation of the total emissivity of the SuperCam LIBS measurements of the soils show a natural break into two groups between 11% and 12% (see Figure S6 in Supporting Information S1). This is similar to the 10% cutoff observed in Cousin et al. (2015), in which values of <10% were interpreted as coarse grains, and >10% were interpreted as fine grained. In this paper, therefore, standard deviations of the total emissivity of <11.5% were interpreted as more likely to be coarse grains, and standard deviations of the total emissivity of >11.5% were interpreted as more likely to be fine-grained soils, and were compared with RMI images.

The LIBS Major-element Oxide Composition (MOC) data comprising the eight most common major elements (Anderson et al., 2022), the H score (Forni et al., 2013), and S and Cl scores (Meslin et al., 2023) averaged for each point (not including the top 5 shots) were analyzed using principal component analysis (PCA) in OriginPro. In order to examine fine grains that might be more likely to form soil crust, coarse grains were removed based on a standard deviation of the total emissivity of >11.5%, as described above. PCA analysis using OriginPro was also performed for selected shot-to-shot data including Naltsos for comparison with the PIXL data.

A special subset of soil surfaces includes soils that were disturbed by the wheel track, including targets Rougon (sol 282), Brandis (sol 302), Chandon (sol 315) and Toudon (sol 333). Points that were disturbed by the wheel tracks were not included in the PCA analysis of the SuperCam points. They were analyzed separately with the SuperCam LIBS Major-element Oxide Composition (MOC) data and H, Cl, and S scores of the disturbed soils Rougon, Chandon, and Toudon averaged and compared to the average of the undisturbed fine-grained soils that are high in H.

2.4.3. Microphone Data

The expansion of the laser-induced plasma is associated with an acoustic signal, which is subsequently recorded by the microphone onboard SuperCam (Maurice et al., 2022) for each of the targets analyzed here. Moreover, recording the laser sparks has been shown to provide data complementary to the LIBS optical spectrum and key information about the target physical properties (Chide et al., 2020, 2021). In particular, it has been shown that for soft targets, the shot-to-shot decrease of the acoustic amplitude is larger since the target is loose. This is due to the excavation of a deep ablation crater and the loss of the laser-matter coupling with depth. Therefore, microphone data are used here to test the cohesion of the soil targets ablated with LIBS and to help discriminate between fine- and coarse-grain soils. Because laser-induced acoustic signal amplitudes are scattered by the turbulence of the Mars atmosphere, shot-to-shot amplitudes are smoothed with a running mean over 3 shots.

The microphone points used in this paper are the same as the LIBS points presented in Table 1. Microphone data are available on the Planetary Data System (Wiens, Maurice, Deen, et al., 2021).

2.4.4. Visible/Near Infrared (VISIR) Spectroscopy

Reflectance spectra in the near-infrared (NIR) were collected by the SuperCam Infrared Spectrometer (IRS) on various soil targets. The IRS consists of an acousto-optic tunable filter spectrometer located in the mast unit of SuperCam and allows the measurement of the near-infrared light in the 1.3–2.6 μm range, in 256 channels and with a spectral resolution of 32 cm^{-1} (Fouchet et al., 2022). In this spectral range, several mineral phases can be detected, owing to overtone vibration of bonds active in the infrared. In particular, this technique is sensitive to the presence of mafic minerals (such as pyroxene and olivine) due to their electronic absorption bands and alteration minerals such as phyllosilicates, carbonates, sulfates, phosphates, zeolites, oxides, etc. (for a review, see Bishop, 2019) due to their overtone vibrational bands in the IR region. Results from the VISIR instrument are reported in Mandon et al. (2023). The calibration of the data is presented in Royer et al. (2023): it consists of a conversion of the raw data into reflectance, a correction of the atmospheric-related absorptions and a correction of the artifacts induced by the thermal sensitivity of the IRS. The field of view of the instrument is 1.15 mrad (Maurice et al., 2021), which corresponds to a footprint of ∼2.3 mm for a mast-to-target distance of 2 m. This implies that, for fine soils where the particle size is less than the diameter of the laser beam (250–350 μm), overall homogeneous materials are observed by the spectrometer. This also implies that the surface measured in VISIR is larger than the LIBS footprint (0.25–0.45 mm; Wiens, Maurice, Robinson, et al., 2021) and that comparison of LIBS and VISIR data might not always be straightforward.

2.5. Examination of Soil Using MEDA

The MEDA instrument is the meteorological package onboard M2020, and it comprises six sensors measuring the environmental conditions across *Perseverance's* traverse (Rodriguez-Manfredi et al., 2021). Among these, the Relative Humidity Sensor (RHS) and the Thermal Infrared Sensor (TIRS) are measuring the relative humidity with respect to ice (RH) at 1.45 m and the ground temperature (Tg) (Sebastián et al., 2021), respectively. Here, RHS and TIRS measurements are used to estimate the relative humidity at the ground with respect to ice (RHg), providing environmental context for the potential formation of frost and changes in the hydration state of salts identified by PIXL and SuperCam.

To calculate RHg, the water vapor pressure (e) at 1.45 m is derived as

$$e = \mathrm{RH} \times e_s(\mathrm{Tb}), \tag{1}$$

where Tb is the board temperature of the RHS and e_s is the saturation vapor pressure over ice (Martínez et al., 2016). Then, RHg is obtained as $\mathrm{RHg} \approx e/e_s$ (Tg), where it has been assumed that the water vapor pressure is constant in the first 1.45 m. We note that potential surface/atmosphere exchanges of H_2O via adsorption/desorption (physisorption), changes in the hydration state of salts (chemisorption), and frost formation would result in departures from a constant vertical profile. Therefore, MEDA results are subject to uncertainties derived from this assumption (Polkko et al., 2023).

This soil-atmosphere water interaction is expected to depend on the temperature of the soil, and the surface relative humidity is calculated using Tg, which is the temperature of the top most soil layer. However, there is a thermal gradient within the top most 15 cm, which is produced by the penetration of the diurnal thermal wave. The upper layers of the soil and rocks will experience large thermal changes whereas a few centimeters below the surface the temperature variation will be milder, and therefore assuming that water molecules traverse the pore-space freely, the relative humidity will also be lower. In summary, we assume that the top most layer will be the one exposed to lower diurnal temperatures, and higher relative humidity values, whereas the soil layers underneath will be exposed to drier conditions at night-time. Because of the existence of this vertical gradient, the hydration of the soil is likely depth-dependent.

3. Results

3.1. Identification of Soil Crusts in Images

Soil crusts were apparent at 45 of 101 rover stops evaluated with Hazcam and Navcam images (Figure 2). Crusts were evident also at two of seven locations where helicopter flights crossed wheel tracks. There was clear evidence of soil crust in four of the eight coring/abrasion locations. These results likely represent an underestimate of the presence of soil crusts in the study area because soil crusts are detected most readily when relatively extensive disturbances occur by the wheels or coring/abrasion activities and can be examined closely (although see also

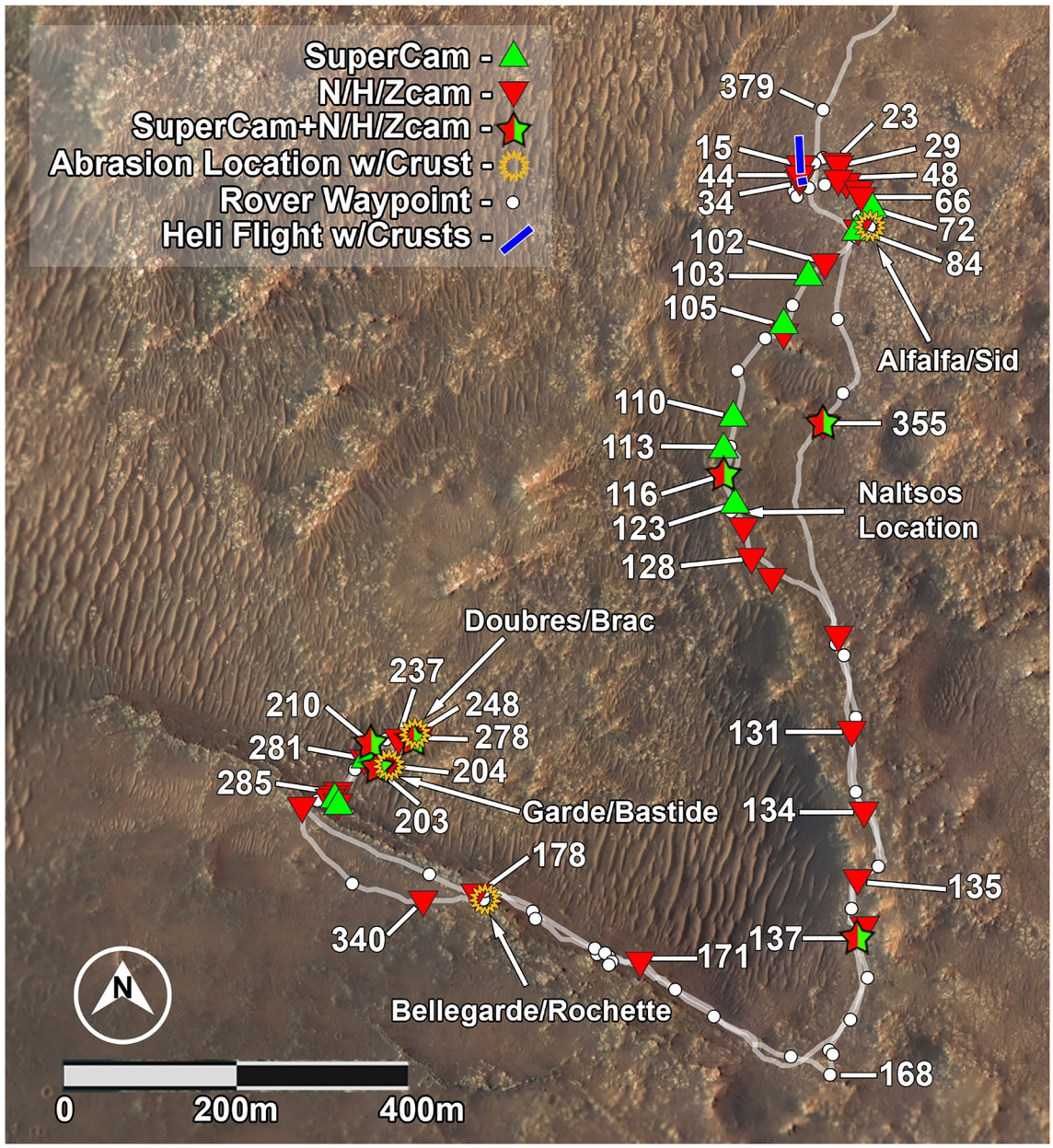

Figure 2. Map (HiRISE Color Basemap, NASA/JPL/University of Arizona) of the rover traverse indicating rover stops (white points), SuperCam analyses (indicated in green), and evidence of crusts observed near wheel tracks (red points/half red stars), by the helicopter (blue lines), at abrasion locations (indicated with orange circles). The Naltsos target measured by PIXL is labeled on the map. The Navcam (Maki et al., 2020b), Hazcam (Maki et al., 2020a) and helicopter (Balaram et al., 2021) images are available in the Planetary Data System (PDS).

Figure S4 bottom in Supporting Information S1, which indicates a disturbed crust not impacted by the rover). These results indicate that the process of crust formation is widespread in the study area on the floor of Jezero crater, consistent with observations at previous landing sites on Mars.

Physical disturbance of the surface on or close to rover tracks demonstrates the presence of soil crusts (Figures 1a, 1c, and 1e), and the 3-D data analysis of stereo images of those features allows quantification of their characteristics (Figures 1b, 1d, and 1f). The height of offsets induced by the soil disturbances varies between 4 and 23 mm. The angles of the slopes in the places where the height was measured are greater than the angle of repose (Atwood-Stone & McEwen, 2013). The length of the discontinuations (perpendicular to slope) over the entire portion is up to 18 cm in one case (Figures 1e and 1f). The depth and shape of the wheel tracks (Figures

in Table S2) with a large fraction of scattered edges, and with large fractions of wheel track areas conforming to the shape of the wheel fins (Figures in Table S2) vary widely, with wheel track depths ranging from 3 to 12 mm (see Table S2). In two locations where the crust was disturbed by the abrasion/coring activities, stereo Mastcam-Z images allowed quantification of the thickness of the crust, with results of 1 and 2 mm thick (Figure S4 in Supporting Information S1). The crusts observed on dunes are typically coarse-grained and the crusts observed in flatter areas are either fine-grained or a mixture of fine and coarse grains (Figure S5 in Supporting Information S1).

3.2. Hydrated Surfaces

An examination of the average H score in shots 6–10 vs. the deepest 10 shots show that most points indicate either (a) a statistically significant decrease from shots 6–10 to the deepest 10 shots (92 points total), or (b) the H score of the surface, even though it does not show a statistically significant decrease, is above the average H score (56 total points), with a few points not corresponding to either of these trends (12 total points). An RMI of the Que_eh_SCAM target with the LIBS-generated soil pits indicated 1–10 is shown in Figure 3a, and the H scores with shot for points 1–10 indicated in Figure 3a are shown in Figure 3b. Figure 3b therefore shows whether or not H scores decrease from the soil surface into the soil, and the most common types of variations in the H score with depth throughout the early mission are shown in Figure 3b. The greatest number of points is on coarse grains with a decrease in the H score from the surface (65 points). A nearly equal number of fine-grained points have H scores that do not decrease from the surface (50 points). A substantial number of points are fine-grained with a decrease in H from the surface (27), and small numbers of fine soils are consistently low in H (7), coarse grains that are consistently high in H (6), and coarse grains that are consistently low in H (5) (Figure 3d). Measurements were all made during the daytime, and hydration may differ at night.

The comparison of the microphone data within the different points in a raster also supports the classification between the fine- and coarse-grain points (see Figure 3c): fine-grain soils on target Queh_eh_SCAM (points #5, #6, #7, and #10) experience a large decrease in the laser-induced acoustic signal amplitude over the burst due to the uniform penetration of the laser in this layer. In contrast, the acoustic signals from coarse-grain soil keep a higher amplitude (points #1, #3, #4), sometimes with variations more complex to interpret, likely due to the laser hitting a mixture of fine grains underlying a larger grain. This is especially the case for point #9 where the acoustic data suggest that the first part of the burst ablated fine soils whereas the last 15 shots ablated a buried grain (see RMI in Figure 3a). Overall, the acoustic classification is consistent with what is seen on the H score (Figure 3d).

An overview of the mineral phases detected during the crater floor campaign on rocks, soils and dust using SuperCam VISIR spectroscopy is provided in Mandon et al. (2023). The mean spectra of two disturbed soils (*Keyah* and *Toudon* targets) and two undisturbed soils (Cheskeh and Queh Eh) compared with laboratory reflectance spectra (Figure 4) indicate hydrated phases in soils, similar to observations from Gale crater (Achilles et al., 2017, 2021; Gabriel et al., 2018). Disturbed soils are similar to other fine soils and exhibit a spectral absorption band in the 1.3–1.7 μm range consistent with the presence of olivine detected from orbit (Brown et al., 2020), which is also strongly associated with coarse-grained material (Vaughan et al., 2023), as has also been observed in Gale crater (Ehlmann et al., 2017). An absorption near 1.9 μm is also observed, a band related to the combination of elongation and bending modes of the water molecule. Additional shallow absorptions at 2.28 (Fe^{3+}–OH) and 2.32 μm (Mg–OH and/or CO_3^{2-}) are observed, indicating that water is present in hydrated mineral phases such as Fe/Mg-phyllosilicates such as nontronite (Turenne et al., 2022) possibly with carbonates; nontronite has also been detected using CheMin at Gale crater (Rampe et al., 2020). These features are also observed in the surrounding rocks (Mandon et al., 2023), possibly indicating a local contribution to the soils. The enlargement of the 1.9 μm band and the blue slope in the 2–2.5 μm range is indicative of the presence of pyroxene inducing a large absorption band centered near 2 μm.

3.3. Examination of Surface Crusts Using PIXL

Apparently cohesive dust on a natural rock surface was observed at the Naltsos target on sol 125. The Naltsos surface has a "dusty" appearance (i.e., pale orange-brown color in Navcam and Mastcam-Z, and irregular, "fluffy" dust aggregates visible in SHERLOC/WATSON microscopic images). The left side of the scanned target

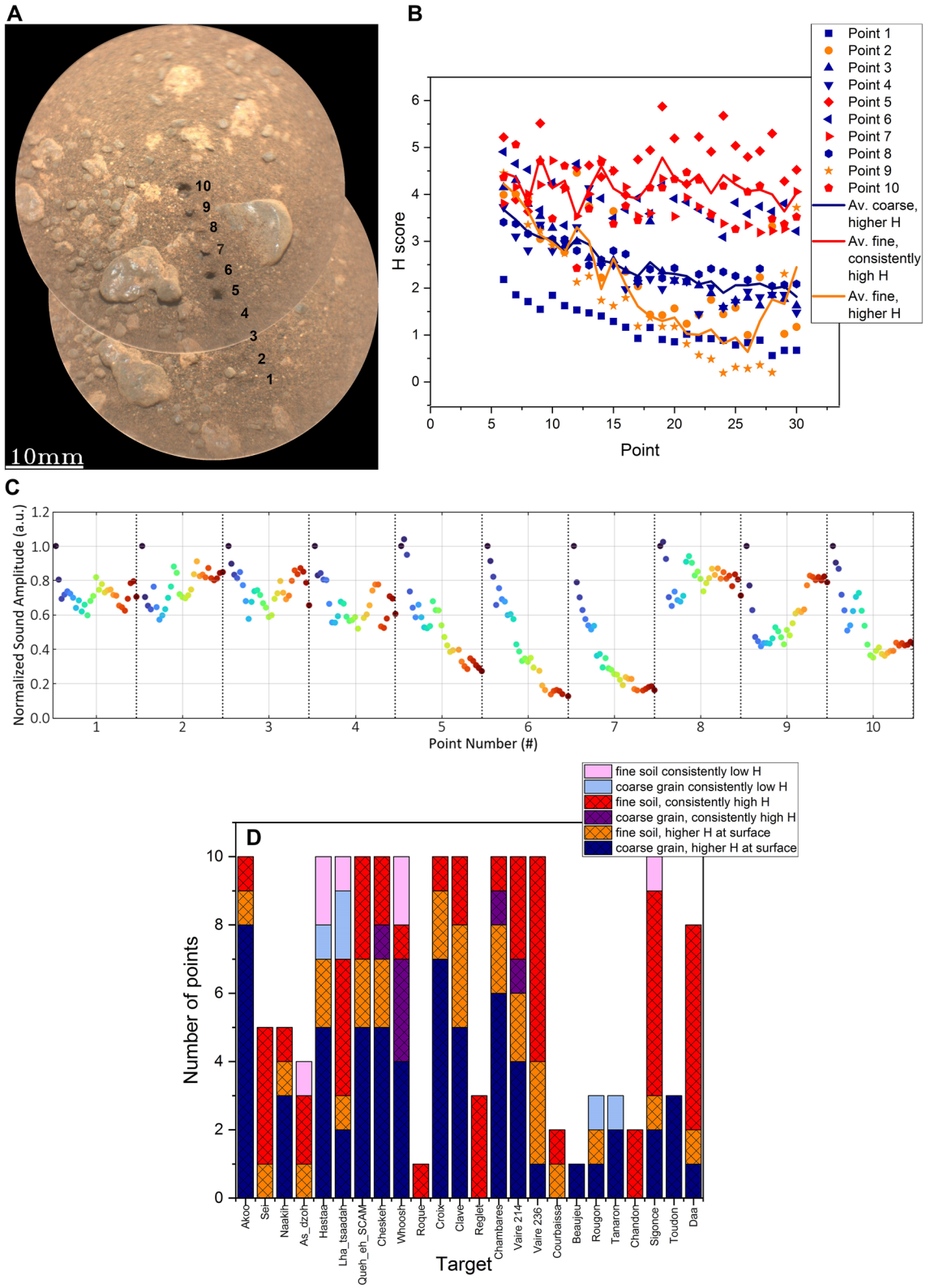

Figure 3.

includes a collection of rounded sand grains that are ~1.5 mm in diameter and visibly coated by dust (Figure 5b). PIXL analysis confirms a significant amount of dust on the Naltsos target. Of the 120 spots, 102 are relatively uniform in major elements and similar to Mars' global airfall dust measured by the *Curiosity* Alpha Particle X-ray Spectrometer (APXS) in Gale crater (Berger et al., 2016), also measured by ChemCam (Lasue et al., 2018). The remaining spots represent partially dust-covered windows to the underlying rock substrate with compositions that are largely mixtures of igneous minerals of the rock (plagioclase feldspar, augite, and an Fe-silicate) or sand grains (Fe-Mg-rich, likely olivine) and airfall dust. Low-lying eolian ripples partially bury the Naltsos outcrop (Figure 5a), which suggests that the relatively recent and likely episodic burial and exhumation from the shallow subsurface by transient bedforms has affected the rock's surface, and the Naltsos surface is composed of a combination of dusty bedrock, a dusty surface, and a dust crust (Figure 5).

The depth of penetration for elements measured by PIXL increases with atomic number for elements accessed with the K edge (Na to Zr). Among the dusty spots on Naltsos, the dust coating is thick, greater than ~50 μm, as indicated by narrow ranges of nonvolatile element concentrations (i.e., $Z < 26$) while the abundances of volatiles in the dusty regions vary spot to spot. Derived Cl values are high (~1.5x) compared to global Mars dust (Berger et al., 2016). Absolute concentrations may be revised as PIXL calibration, in particular Cl, which has a significant background from the Rh anode L line, continues to be verified. Relative differences in volatile element concentrations among the dusty targets are robust (i.e., not attributable to spectral artifacts or X-ray diffraction interference) and the right side of the scan is particularly enriched in SO_3 and Cl (i.e., an elemental signature of Martian dust) compared to dusty spots elsewhere in the scan (Figure 5). This volatile element enrichment is coincident with the surface of the rock with a uniform appearance and ends at a slight step down to the left (indicated by arrows in Figure 5b). The composition of this surface correlates well with the existing literature (i.e., Berger et al., 2016; Yen et al., 2005). It is, however, richer in SO_3 and Cl relative to the thick dust portions of the scan (Figure 5c). This prompts the interpretation of this region of the scan to be indurated dust ("dust crust") with SO_3- and Cl-bearing salt cement. Positive correlations between Mg and SO_3 (Figure 5e) suggest the presence of Mg-sulfate.

PIXL contains two detectors ("A" and "B"). Through the comparison of X-ray spectra from each of the detectors, the dust and dust crust may be understood further. Multiple diffraction peaks are observed in the dusty bedrock spectra, suggesting that well-ordered and crystalline igneous minerals are present in the rock substrate (Liu et al., 2022). Conversely, spectra for "dust crust" and thick dust are identical and do not contain X-ray diffraction peaks (Figure 5). The "dust crust" and surface airfall dust is therefore interpreted as being less crystalline (i.e., more amorphous), indicating a <45 μm grain size and overall amorphous characteristics of both the surface dust and cementing agent in the "dust crust" (Tice et al., 2022), and may be similar to surface coatings observed in Jezero crater (Garczynski et al., 2022).

The chemistry of "thick dust" is a good match to the composition of Martian global soil (e.g., Berger et al., 2016). The Gale dust-normalized (Berger et al., 2016) element abundance diagram for Naltsos dusty bedrock, Fe-Mg-rich

Figure 3. (a) Remote microimager (RMI) mosaic of Que_eh_SCAM, showing the location of the pits formed by the LIBS shots. The early shots are difficult to discern, possibly because the holes were filled by the excavation of the following shots, or because the size of the grains was different and they collapsed, or because there are small pebbles buried that prevent digging in the soil or a combination of all of these factors. Each pit is labeled 1–10. (b) Image showing the decrease of H with depth from the surface of Que_eh_SCAM, which contains the most common types of grains; points 1–10 correspond to the points 1–10 in panel (a), and the average of each of the different types of points (blue = coarse grain, higher H at the surface; red = fine soil, consistently high H at the surface, and orange = fine soil, higher H at the surface). (c) Evolution of the amplitude of the laser-induced acoustic signal (normalized by the first shot of each burst) for the 10 points of Queh_eh_SCAM. Each panel records 30 laser shots; the color code, from dark blue to dark red, indicates the number of the shots for a burst. (d) Breakdown of points by low variation in emissivity (more indicative of a coarse grain), and higher variation in emissivity, and a decrease in H from the surface, versus more constant, higher and lower H scores at the surface. The greatest number of points (65) are coarse grains with a decrease in the H score from the surface (points from samples A_koo, Naakih, Hastaa, Lha_tsaadah, Que_Eh_SCAM, Cheskeh, Whoosh, Croix, Clave, Chambares, Vaire 214 and 236, Beaujeu, Rougon, Tanaron, Sigonce, Toudon, and Daa). A nearly equal number of fine-grained points (50) contain H scores that do not decrease from the surface (points from samples Akoo, Sei, Naakih, As_dzoh, Lha_tsaadah, Que_Eh_SCAM, Cheskeh, Whoosh, Roque, Croix, Clave, Reglet, Chambares, Vaire 214 and 236, Courbaissa, Chandon, Sigonce, and Daa). A smaller, but still substantial number of points (27) are fine-grained with a decrease in H from the surface (points from samples Akoo, Sei, Naakih, As_dzoh, Hastaa, Lha_tsaadah, Que_Eh_SCAM, Cheskeh, Croix, Clave, Chambares, Vaire 214 and 236, Courbaissa, Rougon, Sigonce, and Daa). Finally, a small number of points do not follow any of these trends, and instead are fine soil that are consistently low in H (seven points from samples As_dzoh, Hastaa, Lha_tsaadah, Whoosh, and Sigonce), coarse grains that are consistently high in H (six from samples Cheskeh, Whoosh, Chambares, and Vaire 214), and coarse grains that are consistently low in H (five points from samples Hastaa, Lha_tsaadah, Rougon, and Tanaron). The points in B are color-coded to correspond to the most common types of grains observed throughout the mission: coarse grains with a decrease in H score = blue, fine grains with a consistently high H score = red, and fine grains with a decrease in H score = orange. The SuperCam H scores are generated after Forni et al. (2013), and the retrieved H component used to tabulate the H scores after Forni et al. (2013) is included in Figure S7 of Supporting Information S1 and Table S1. The SuperCam total emissivity data are included in the Planetary Data System (Wiens, Maurice, Deen, et al., 2021).

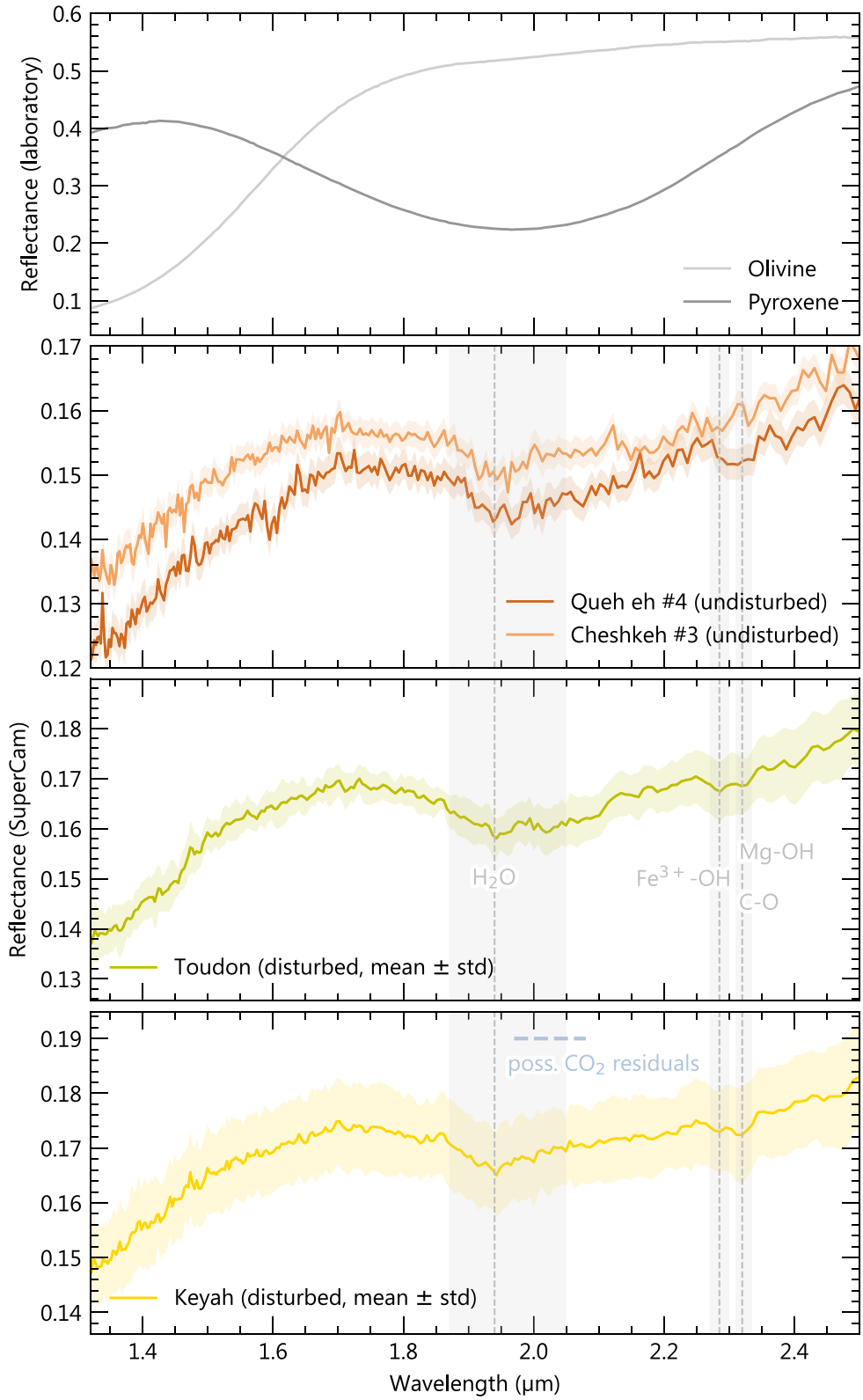

Figure 4. Mean reflectance spectra of two undisturbed fine soils (Qeh_Eh and Cheskeh), and two disturbed soils (Keyah and Toudon) observed during the first year of the mission and measured by the IRS, compared with laboratory reflectance of the RELAB library (olivine C1PO47, pyroxene CASB52; Pieters & Hiroi, 2004). All SuperCam raw data and processed calibrated data files are included in the Planetary Data System (Wiens, Maurice, Deen, et al., 2021).

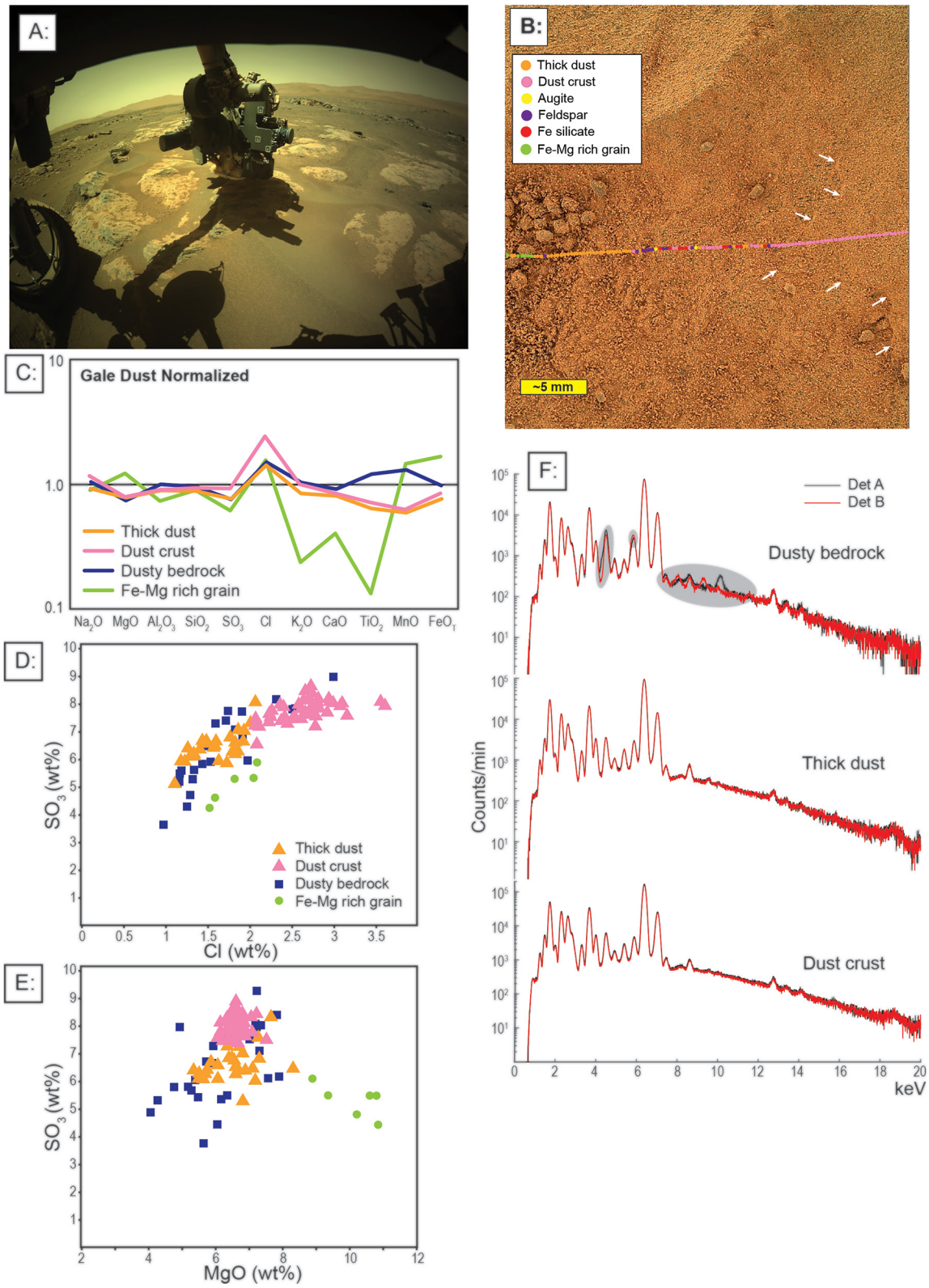

Figure 5.

Table 2
Major-Element Oxides in wt%, Cl, H, and S Scores for the Disturbed Soils and Fine-Grained Soils High in H

		SiO_2	TiO_2	Al_2O_3	FeOT	MgO	CaO	Na_2O	K_2O	Cl score	H score	S score
Disturbed	Avg (5)	37.6	1.05	7.91	16.1	7.2	5.3	1.79	1.03	0.0045	3.1	0.43
	SD	8.5	0.63	0.72	4.4	2.2	3.3	0.29	0.59	0.0045	1.4	0.27
Undisturbed	Avg (59)	44.6	0.68	7.3	16.9	10.2	4.04	1.69	0.68	0.013	4.0	0.53
	SD	2.3	0.25	1.8	6.3	6.6	0.82	0.51	0.40	0.016	1.0	0.15

Note. SD = standard deviation.

sand, thick dust, and dust crust is shown in Figure 5c. As has occurred elsewhere, local soils can reflect an exceptionally close approximation to global soil, albeit sometimes with minor influence from local igneous rocks and sediments. Contributions to the local soil by Jezero rocks with their high Fe content (Liu et al., 2022) are evidenced by the somewhat higher Fe in the "thick dust," which also reduces the apparent SiO_2 abundance (all concentrations have been normalized to 100 wt% total). The thick dust material is at the high end of the sulfate content for global soils (e.g., Berger et al., 2016; Yen et al., 2005), but has much higher chlorine content, which also reflects the surprisingly higher Cl content of Jezero rock (Tice et al., 2022).

3.4. Correlation of Elements in Analyses by SuperCam

PCA analysis of the averaged shots for each SuperCam LIBS point shows that H, Cl, and S are tightly correlated (Figure 8). These results suggest the presence of hydrated salts that may be contributing to the formation of the soil crusts, similar to the results observed by PIXL. For specific comparison with the PIXL measurements, PCA analysis of the shot-to-shot SuperCam data on Naltsos indicates tight correlation of Mg with H, suggesting that the Mg sulfates observed by PIXL might be hydrated (Figure S3 in Supporting Information S1).

A comparison of the averaged Major-element Oxide Composition (MOC) and S, Cl, and H scores of the disturbed soils Rougon, Chandon, and Toudon with the average of the undisturbed fine-grained soils that are high in H indicates that the chemistry of the soils are within one standard deviation (Table 2).

3.5. Examination of Soil Using MEDA

Pairs of RHg and Tg values estimated from MEDA for the first 423 sols of the M2020 mission, along with superimposed lines representing stable (solid) and metastable (dashed) boundaries for the $MgSO_4.nH_2O$ and $CaSO_4.nH_2O$ systems (Chou & Seal, 2007) (Figure 6) show that, should kinetics allow (Fischer et al., 2019; Rivera-Valentín et al., 2020), these salts might undergo changes in their hydration state over diurnal cycles. Although not shown, the environmental conditions at the surface are not favorable for the deliquescence of any known pure salt on Mars. However, saturated conditions on the ground might have been achieved on sols 105, 107 and 282 (Figure 7). In each of these sols, the terrain "seen" by the field of view of TIRS was comprised of fine-grained material with relatively low thermal inertia (Martínez et al., 2023), which results in colder overnight surface temperatures. In these soils, because they are not disturbed by the wheel tracks or by abrasion/coring activities, fractured or "rafted" crusts are not observed, but that does not mean that they are not present.

4. Discussion

In this manuscript, we examine soil crust characteristics, potential formation mechanisms, and implications for the history, potential past habitability, and future human exploration of Mars. Evidence for soil crust includes

Figure 5. (a) Sol 125 front Hazcam image of the PIXL instrument deployed on the Naltsos bedrock target. (b) SHERLOC Watson image of the Naltsos bedrock target, modified to enhance the appearance of dust by methods presented in Schmidt et al. (2018) with the PIXL line scan shown. (c) Gale dust-normalized (Berger et al., 2016) element abundance diagram for Naltsos dusty bedrock, Fe-Mg-rich sand, thick dust, and dust crust. (d) Plot of SO_3 versus Cl (wt%) to illustrate the enrichment in SO_3 and Cl in the dust crust relative to the airfall dust. (e) Plot of SO_3 versus MgO (wt%) show the correlation between SO_3 and MgO in the thick dust, dust crust, and dusty bedrock, and not in the Fe-Mg-rich grains (f) PIXL A (black) and B (red) X-ray spectra for dusty bedrock, thick dust, and dust crust. Count discrepancies between A and B (highlighted in gray) are the product of the superposition of X-ray diffraction on the X-ray fluorescence spectra in dusty bedrock. A lack of spectral differences in the thick dust and dust crust indicates that they are amorphous to PIXL (cf., Tice et al., 2022). The PIXL images and spectra are in the Planetary Data System (PDS) (Allwood & Hurowitz, 2021), and the oxide concentrations are in Table S3 of Supporting Information S1. For a comparison with other Mars soils, see Figure S2 in Supporting Information S1.

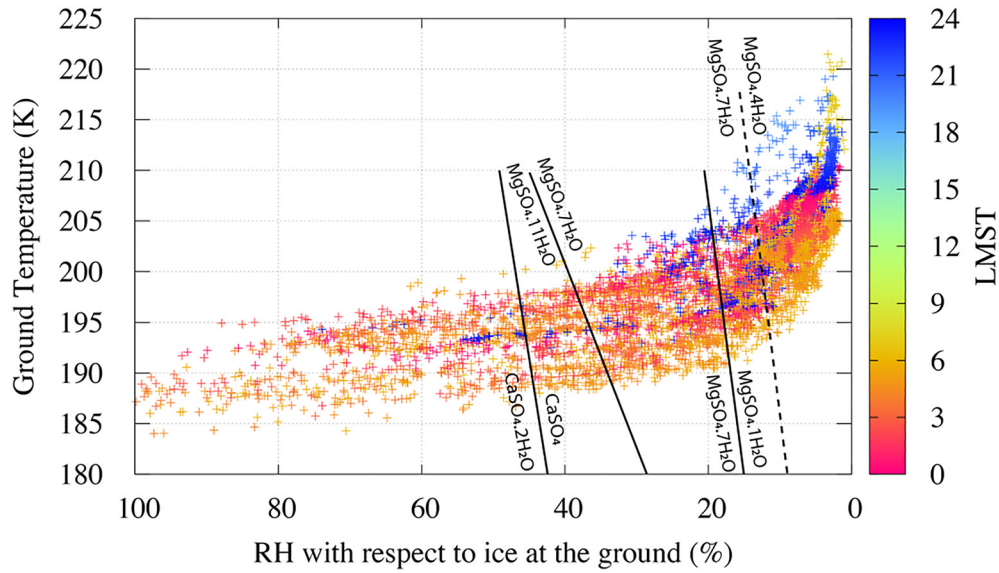

Figure 6. Ground temperature versus relative humidity at the ground and local mean solar time (LMST) (color bar) for the first 423 sols of the M2020 mission, with superimposed lines representing stable (solid) and metastable (dashed) boundaries for the $MgSO_4.nH_2O$ and $CaSO_4.nH_2O$ systems. Results indicate that salts present in the Martian regolith might undergo changes in their hydration state under current conditions at Jezero. Although not shown, the environmental conditions at the ground are not favorable for the deliquescence of pure salts on Mars. However, values of RHg >100% have been achieved on certain sols, suggesting that frost formation might be possible. Only pairs of RH and Tg values for which measured RH at 1.45 m is above 2% are shown here. This is because RH values below 2%, which are typically acquired during the daytime, although known to be less than 2%, cannot be known more precisely than that. This limits the coverage of this figure to LMST mostly between 00:00–08:00 and 20:00–24:00, with no measurements whatsoever shown from between 11:00 and 18:00. All Mars 2020 MEDA data necessary to reproduce each figure shown in this manuscript are available via the Planetary Data System (PDS) Atmospheres node (Rodriguez-Manfredi & de la Torre Juarez, 2021).

fracturing and "rafting" of the surface (Figure S1 in Supporting Information S1), which has been previously widely observed on Mars (e.g., Arvidson et al., 2010; Blake et al., 2013; Brückner et al., 2003; Clark et al., 1982; Sullivan et al., 2011). The soil crust is more cohesive than the subsurface material; subsurface cohesion is observed in increased angles of repose and shallower track depths observed by Mastcam-Z (Figure 1 and Table S2). Cohesion can be caused by the presence of liquid water, the presence of salts, as well as characteristics of the grains themselves such as grain size or grain morphology. The fine-grained material present beneath the surface observed in the wheel tracks may therefore be contributing to this evidence of subsurface cohesion. The fine-grained material beneath the surface was likely transported over long distances, and thus impacted by geochemical processes occurring at the Martian surfaces, both at Jezero crater and in other locations.

Evidence of soil crusts was widely observed during the traverse across the Jezero crater floor in Hazcam and Navcam images of the wheel tracks in 45 out of 101 rover stops, two flights from the helicopter out of seven that crossed the rover wheel tracks, as well as clear evidence in four out of the eight coring/abrasion locations (Figure 2). Evidence of soil crusts is therefore prevalent at Jezero crater, and their formation mechanisms are important for understanding the surface of Mars.

To better understand the characteristics of the soil crust and the subsurface cohesion, measurements of the soil crust and the soil excavated by wheel tracks by SuperCam, and measurements of the target Naltsos by PIXL, were examined. Examination of the LIBS shot-to-shot data indicated characteristically higher H scores at the soil surface (Figures 3b and 3d). Comparing the changes in H scores to estimates of grain size based on the standard deviation of the total emissivity, SuperCam LIBS H scores of the fine soils are most commonly observed to be consistently high (50 points), but with a substantial number of points that show a decrease from the surface (27 points). This suggests that the thickness of the hydrated crust is in more cases thicker than the depth of the pits generated by the SuperCam LIBS (likely 1–2 mm, Meslin et al., 2013), but in some cases less than this thickness. This potential thickness of the crust (1–2 mm) is consistent with measurements of the thickness of the crust from 3D data analysis of the Mastcam-Z stereo images (Figure S4 in Supporting Information S1), which indicate

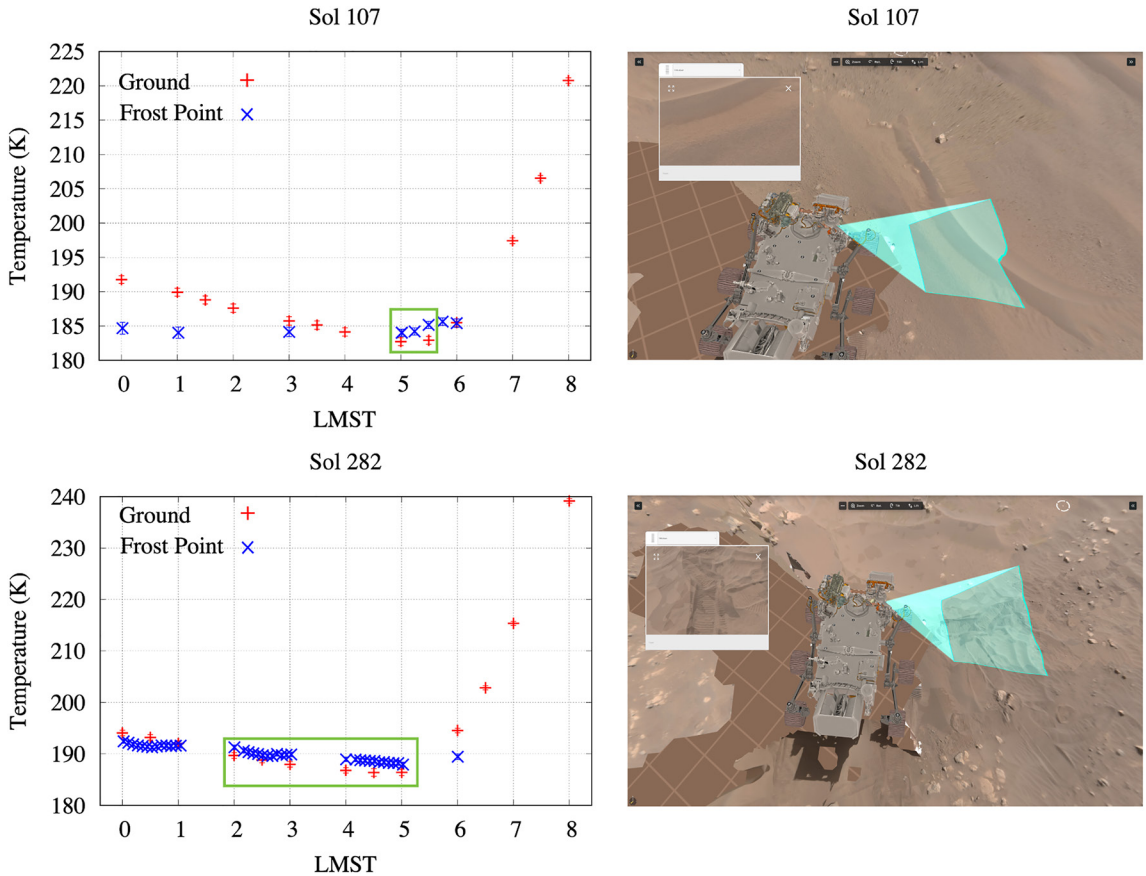

Figure 7. Potential frost events at Jezero crater. (top) Observed ground temperature (red) and estimated frost point temperature (blue) on sol 107 as a function of local mean solar time (left), and TIRS' field of view of the corresponding terrain (right). (bottom) Same as above but for sol 282. Potential frost events occur when the ground temperature falls below the frost point (green boxes). These events have been identified only for a few sols when the thermal inertia of the terrain was relatively low (fine-grained material), resulting in colder overnight ground temperatures. All Mars 2020 MEDA data necessary to reproduce each figure shown in this manuscript are available via the Planetary Data System (PDS) Atmospheres node (Rodriguez-Manfredi & de la Torre Juarez, 2021).

thicknesses of the crust disturbed during the coring and abrasion activities of 1 and 2 mm. These estimates are also comparable to previous work measuring soil crust thicknesses of a few mm at other sites (Sullivan et al., 2011).

The consistently high H values commonly observed with SuperCam LIBS for the fine-grained soils (Figure 3d) are also consistent with measurements by the SuperCam VISIR that measure a 1.9 μm H_2O band depth for the fine-grained samples, including specifically Toudon, Keyah, Que Eh, and Cheskeh (Figure 4). The observation of the 1.9 μm H_2O VISIR band depth together with the LIBS H score suggests that the presence of H_2O is contributing to the H score measured by LIBS.

To examine the chemical characteristics of this potentially hydrated soil crust, PCA analysis was performed on the Major-element Oxide Composition (MOC) values (Anderson et al., 2022) together with the H (Forni et al., 2013), Cl, and S (Meslin et al., 2023) LIBS scores. The correlation (indicated by the small angles between the loading vectors) of the H, Cl, and S scores, separated from a correlation of Fe and Mg, and K, Ca, Al, and Na (Figure 8) suggest evidence for crusts on two different types of grains, more mafic grains and more felsic grains.

PIXL analyses of the surface of the Naltsos target indicate a correlation between Mg and S (Figure 5e), suggesting the presence of Mg-sulfates. For comparison, PCA analysis of the shot-to-shot SuperCam data on Naltsos indicates tight correlation of Mg with H for the SuperCam points measured on Naltsos (Figure S3 in Supporting Information S1), suggesting that the Mg sulfates observed by PIXL are likely hydrated. This observation is consistent with previous data indicating that amorphous sulfates are the primary carriers of hydration at Gale crater, Mars (David et al., 2022).

Both SuperCam and PIXL data suggest the presence of salts that are likely contributing to the cohesion of soil particles and therefore the formation of crusts, as well as cohesion beneath the surface. Soil crusts on Earth can

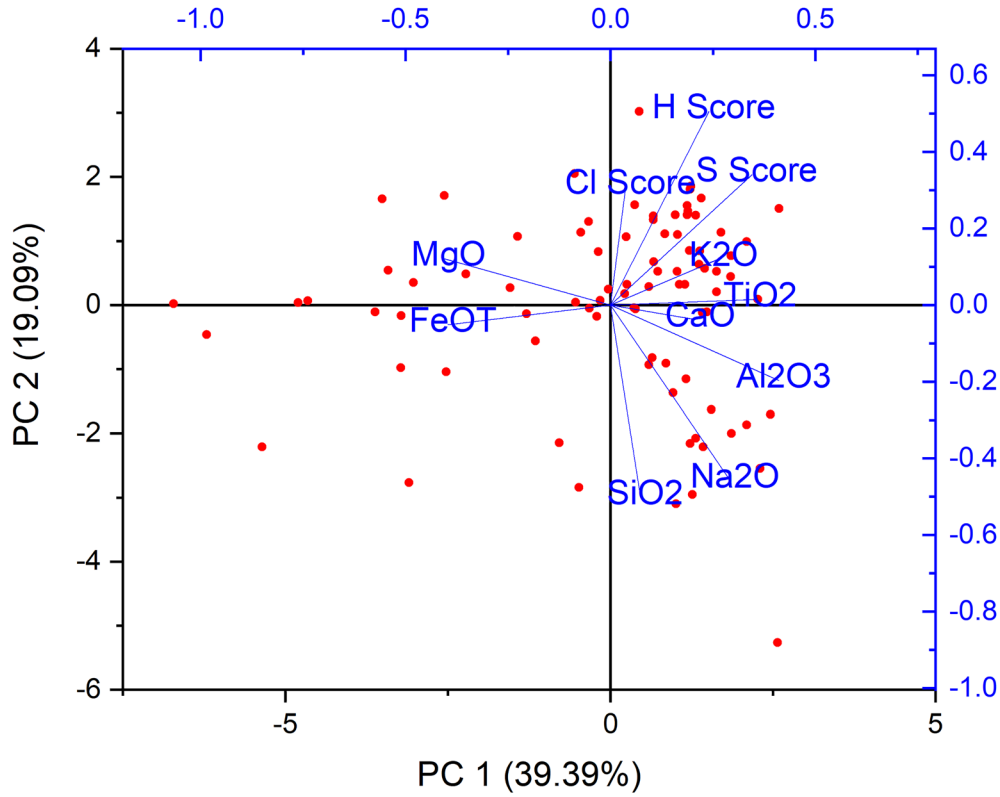

Figure 8. PCA analysis using OriginPro of the averaged shot data for the Major-element Oxide Composition (MOC) values compared to H, S, and Cl scores for points that are fine-grained (i.e., likely contain soil crust). PCA analysis shows the correlation of H, S, and Cl, which suggests the potential presence of hydrated salts. The SuperCam Major-element Oxide Composition (MOC), total emissivity, and all raw data and processed calibrated data files are included in the Planetary Data System (Wiens, Maurice, Deen, et al., 2021). The SuperCam H scores are generated after Forni et al. (2013), and the retrieved H component used to tabulate the H scores after Forni et al. (2013) is included in Figure S7 of Supporting Information S1 and Table S1. The Cl and S scores are generated after Meslin et al. (2023), and displayed in that manuscript. The vectors represent the loadings in PC1 and PC2, and the points represent the scores of the samples in PC1 and PC2.

form both from wicking of groundwater and atmospheric deposition (Figure 9), and likely both processes, if occurring on Mars, would also form crusts. Terrestrial experiments also suggest that salt crusts can be impacted by saltating particles (Singer & Shainberg, 2004), and thus transport of past salty crusts might also contribute to the atmospheric component of present-day salt crust formation.

Martian soils have very low thermal inertia (as low as 200 TI as measured by MEDA, see Martínez et al., 2023) and therefore the surface soil layer is exposed on a daily basis to large thermal changes, which in turn also produce big variations in the surface relative humidity. When temperatures drop at night, the relative humidity at the surface increases, and atmospheric water may be captured as salts present in the soil absorb and release the water, changing their hydration state. Water may also be absorbed to grain boundaries. Recent experiments with regolith simulant have demonstrated that a mixture containing 10 wt% ferric sulfate can absorb as much as 18% of its weight in water, and a mixture containing 10 wt% calcium chloride can absorb as much as 50% of its weight in water (Ramachandran et al., 2021). In these experiments, this water absorption changes the cohesiveness of fine regolith particles, forming granular structures. The importance of this process of hydration and dehydration, rather than the addition of salts, may be supported by the comparison of the chemical composition of the undisturbed surface and the wheel tracks, which are within one standard deviation (Table 2), but further analyses would be valuable to test this hypothesis.

Therefore, atmospheric water interacting with salts on the surface of Mars likely changes the cohesiveness of the grains at the soil surface, allowing it to form a crust. In addition, frost events (Figure 7) may result in thin films of water that may persist for a few hours (Ramachandran et al., 2021), also increasing cohesion. The fact that the atmospheric and surface temperature conditions at Jezero crater are close to the conditions that would allow

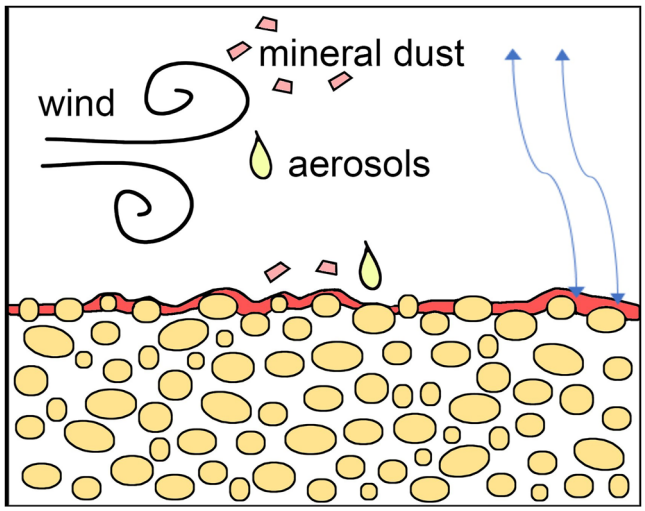

Figure 9. A conceptual figure showing the potential formation of the Jezero crater crusts from atmospheric deposition of both mineral dust and aerosols, followed by hydration and dehydration of the salts. The red crust likely consists of multiple minerals, both detrital and authigenic, such as sulfates, carbonates, nitrates, and chlorides/perchlorates.

the deliquescence of the salts to form brines, which can also cause crusts (Ramachandran et al., 2021), suggests that this process may have been important during the recent past during times of greater obliquity.

Over the course of Martian history, therefore, crusts have likely formed in multiple ways, forming important potentially habitable environments, and have been broken and transported and contributed to the formation of younger crusts. Here in Jezero crater, the surfaces of the soils show a correlation between sulfur, chlorine, and hydrogen, suggesting the availability of these ions to form salts. Experimental work has shown the sorption of phosphate and sulfate onto nanophase weathering products in aqueous solutions (Rampe et al., 2016), suggesting that the sorption of sulfate onto nanophase weathering products in aqueous solutions could be a mechanism for their deposition. S and Cl could also be deposited on dust particles, and result from atmospheric deposition. The observations documented in this manuscript, therefore, are consistent with the formation of the soil crusts at Jezero crater by hydration of salts with changes in relative humidity and potential frost events, cementing the surfaces together. Further work is needed to examine soil crusts throughout the M2020 mission to determine whether soil crusts, including duricrusts, in other locations might result from the presence of groundwater or ice melting, as has recently been documented at the Zhurong landing site (Yang et al., 2022). Lithobiotic microorganisms can live in Ca-sulfate crusts in extremely arid parts of the Atacama Desert (Wierzchos et al., 2011). Microorganisms and other organic matter in shallow groundwater can be wicked to the surface during efflorescence, and salt crusts can also form on top of microbialites (e.g., Cloutis et al., 2021). Salt crusts on Mars may therefore have been a potential environment for long-term survival of past life on Mars, and understanding their formation mechanisms is critical to our understanding of the history of Mars.

5. Conclusions

Soil crusts on Mars are important for understanding both past surface processes as well as the characteristics of the soil that future human explorers will interact with and that will be contained within returned sample tubes. This study examines soil crusts in Jezero crater, and soil crusts have also been broadly observed across Mars at locations including the Viking 1 Landing site, the landing sites of the Mars Exploration Rovers, and the Mars Science Laboratory *Curiosity*.

Soil crusts, which are generally detected when they are disturbed such as by a rover wheel or rock abrasion or drilling, are prevalent across Jezero crater, located in 45 of 101 locations where the soil surface was disturbed by the rover wheels and imaged by the rover's Hazcam, Navcam, or Mastcam-Z cameras; two of the seven helicopter flights that crossed the wheel tracks; and 4 of the 8 abrasion/drilling locations. The surfaces of the soils are hydrated, with the majority of the soil points measured by SuperCam LIBS either showing a statistically significant decrease in hydrogen with depth below the surface, or a consistently high hydrogen score at the surface. Fine-grained soils that generally show a high hydrogen score also show a VISIR 1.9 μm H_2O band. PIXL and SuperCam observations both indicate the presence of salts on the surfaces of the rocks and soils. The specific correlation between magnesium and sulfur (Figure 5) is observed by PIXL in the Naltsos target, and PCA analysis of the shot-to-shot SuperCam data on Naltsos indicate tight correlation of Mg with H, suggesting that the Mg sulfates observed by PIXL are likely hydrated. The potential presence of hydrated Mg-sulfates is also supported by MEDA measurements that indicate that atmospheric humidity and temperature measurements allow the persistence of hydrated Mg-sulfates (Figure 6) as well as frost events (Figure 7). Soil crusts at Jezero crater may therefore be formed by salts at the soil surface that are hydrated by changes in relative humidity and potential frost events, cementing the surfaces together.

Future human missions to Mars are likely to disturb this crust and therefore mobilize its components. Understanding the character of the soil crust is critical for being able to understand the impact of these potential human interactions as well as the returned soil samples, which will likely collect samples of the soil crust that will then

be homogenized as part of sampling. In addition, understanding the formation processes of these soil crusts can help understand when their presence indicates past potentially habitable environments. Further work is therefore needed to examine soil crusts throughout the *Perseverance* mission.

Conflict of Interest

The authors declare no conflicts of interest relevant to this study.

Data Availability Statement

The data in this publication are from the SuperCam, PIXL, Mastcam-Z, MEDA, and Watson instruments, and the Navcam and Hazcam cameras of the Mars 2020 Perseverance rover. The SuperCam data include the Laser Induced Breakdown Spectroscopy (LIBS), Visible/near infrared (VISIR) Spectroscopy, and the Remote Micro-imager images. The PIXL data include images, PIXL spectra, and oxide concentrations. The Mastcam-Z data include the stereo images, and the results of the 3-D processing presented in Paar et al. (2023). The Hazcam and Navcam data include the images, and the MEDA data include ground temperature, relative humidity, and images. The SuperCam Major-element Oxide Composition (MOC), total emissivity, and all raw data and processed calibrated data files are included in the Planetary Data System (Wiens, Maurice, Deen, et al., 2021). The SuperCam H scores are generated after Forni et al. (2013), and the retrieved H component used to tabulate the H scores after Forni et al. (2013) is included in Figure S7 of Supporting Information S1 and Table S1. The Cl and S scores are generated after Meslin et al. (2023), and displayed in that manuscript. The PIXL images and spectra are in the PDS (Allwood & Hurowitz, 2021), and the oxide concentrations are in the supplemental online material (Table S3 in Supporting Information S1). The Mastcam-Z data for all images used in this manuscript are available in the PDS (Bell et al., 2021, https://doi.org/10.17189/BS6B-4782). All Mars 2020 MEDA data necessary to reproduce each figure shown in this manuscript are available via the Planetary Data System (PDS) Atmospheres node (Rodriguez-Manfredi & de la Torre Juarez, 2021). The Navcam (Maki et al., 2020b), Hazcam (Maki et al., 2020a, https://doi.org/10.17189/282b-1524) helicopter (Balaram et al., 2021) and Watson images (Beegle et al., 2021) are available in the PDS. Microphone data are available on the Planetary Data System (Wiens, Maurice, Deen, et al., 2021). The data for comparison from the Mars Exploration Rover mission used in Figure S2 in Supporting Information S1 are available on the PDS for that mission here: https://pds-geosciences.wustl.edu/missions/mer/mer_apxs_oxide.htm.

Acknowledgments
We would like to thank the Mars2020 Science and Engineering teams for their work supporting the mission that has enabled the scientific research presented in this manuscript. We would also like to thank Editor Brad Thomson, reviewer Vincent Chevrier, and one anonymous reviewer for very helpful comments that greatly improved the manuscript. Any use of trade, firm, or product names is for descriptive purposes only and does not imply endorsement by the U.S. Government. E.M. Hausrath and C.T. Adcock acknowledge funding from NASA RSS PS 80NSSC20K0239, K. Benison from NASA Grant # 80NSSC20K0235, J. Christian from NASA PSP 80NSSC21K0328, E. Cloutis from NSERC (RGPIN-2021-02995; RTI-2020-00157), Canadian Space Agency (22EXPCOI4), T.S.J. Gabriel from the Mars 2020 mission, F. Gómez from the Spanish Agencia Estatal de Investigación (AEI), Grant MDM-2017-0737 (Unidad de Excelencia "María de Maeztu"-Centro de Astrobiología INTA-CSIC) and the project DAXE from INTA (Spanish Ministerio de Defensa), J. Johnson from ASU 1511125/15-707; JPL 1532432, A. Knight from NASA PSP 80NSSC21K0328, J.M. Madariaga and J. Huidobro from Project RamOn-Mars, Grant, PID2019-107442RB-C31, Spanish Agency for Research (AEI), G. Martinez wants to acknowledge JPL funding from USRA Contract Number 1638782, T.H. McConnochie from NASA PSP 80NSSC21K0490, M-P. Zorzano from the Spanish Ministry of Science and Innovation (PID2019-104205GB-C21), H.E. Newsom from the Institute of Meteoritics, University of New Mexico, and JPL Subcontract 1395929, G. Paar and A. Bechtold from ESA PRODEX Contract 4000117520, S. Siljeström from the Swedish National Space Agency (contracts 137/19 and 2021-00092), M.E. Schmidt and T. Kizovski from CSA M2020 PSP Grant to Schmidt, S. Schröder from Deutsches Zentrum für Luft- und Raumfahrt (DLR), M.A. Sephton from UK Space Agency (ST/V002732/1 & ST/V006134/1), R. Sullivan from the Mars 2020 mission, A. Udry from NASA PSP 80NSSC21K0330, S. VanBommel from NASA PSP 80NSSC21K0328, R.C. Wiens from JPL Subcontract #1681089. The French authors were supported by CNES, and a portion of the research was carried out at the Jet Propulsion Laboratory, California Institute of Technology, under a contract with the National Aeronautics and Space Administration (80NM0018D0004).

References

Achilles, C. N., Downs, R. T., Ming, D. W., Rampe, E. B., Morris, R. V., Treiman, A. H., et al. (2017). Mineralogy of an active eolian sediment from the Namib dune, Gale crater, Mars. *Journal of Geophysical Research: Planets*, *122*(11), 2344–2361. https://doi.org/10.1002/2017je005262

Achilles, C. N., Morris, R. V., Rampe, E. B., Gabriel, T. S. J., Ming, D. W., Sutter, B., et al. (2021). Factors influencing the formation and preservation of X-ray amorphous materials identified in sedimentary deposits at Gale crater, Mars. In *Lunar and Planetary Science Conference* (Vol. 52).

Allwood, A. C., & Hurowitz, J. A. (2021). Mars 2020 Perseverance Rover PIXL Raw and Derived Data Products. https://doi.org/10.17189/1522645

Allwood, A. C., Wade, L. A., Foote, M. C., Elam, W. T., Hurowitz, J. A., Battel, S., et al. (2020). PIXL: Planetary Instrument for X-Ray Lithochemistry. *Space Science Reviews*, *216*(8), 134. https://doi.org/10.1007/s11214-020-00767-7

Anderson, R. B., Forni, O., Cousin, A., Wiens, R. C., Clegg, S. M., Frydenvang, J., et al. (2022). Post-landing major element quantification using SuperCam laser induced breakdown spectroscopy. *Spectrochimica Acta Part B: Atomic Spectroscopy*, *188*, 106347. https://doi.org/10.1016/j.sab.2021.106347

Arvidson, R. E., Ahsley, J. W., Bell, J. F., III, Chojnacki, M., Cohen, J., Economou, T. E., et al. (2011). Opportunity Mars Rover mission: Overview and selected results from Purgatory ripple to traverses to Endeavour crater. *Journal of Geophysical Research*, *116*, E00F15. https://doi.org/10.1029/2011JE003746

Arvidson, R. E., Bell, J. F., III, Bellutta, P., Cabrol, N. A., Catalano, J. G., Cohen, J., et al. (2010). Spirit Mars Rover Mission: Overview and selected results from the northern Home Plate Winter Haven to the side of Scamander crater. *Journal of Geophysical Research*, *115*, E00F03. https://doi.org/10.1029/2010JE003633

Atwood-Stone, C., & McEwen, A. S. (2013). Avalanche slope angles in low-gravity environments from active Martian sand dunes. *Geophysical Research Letters*, *40*(12), 2929–2934. https://doi.org/10.1002/grl.50586

Aubrey, A., Cleaves, H. J., Chalmers, H. J., Skelley, A. M., Mathies, R. A., Grunthaner, F. J., et al. (2006). Sulfate minerals and organic compounds on Mars. *Geology*, *34*(5), 357–360. https://doi.org/10.1130/G22316.1

Balaram, J., Deen, R. G., Algermissen, S., Dunn, A. E., Toole, N. T., Crombie, K. M., et al. (2021). Mars 202 Perseverance Rover Helicopter Camera Suite Experiment Data Record (EDR) and Reduced Data Record (RDR) Data Products. https://doi.org/10.17189/1522845

Bao, H., Jenkins, K. A., Khachaturyan, M., & Díaz, G. C. (2004). Different sulfate sources and their post-depositional migration in Atacama soils. *Earth and Planetary Science Letters*, *224*(3–4), 577–587. https://doi.org/10.1016/j.epsl.2004.05.006

Beegle, L. W., Bhartia, R., Deen, R. G., Padgett, D., Algermissen, S., Dunn, A. E., et al. (2021). Mars 202 Perseverance Rover SHERLOC Raw, Partially Processed and Derived Data Products. https://doi.org/10.17189/1522643

Bell, J. F., III, Maki, J. N., Mehall, G. L., Ravine, M. A., Caplinger, M. A., Bailey, Z. J., et al. (2021). The Mars 2020 Rover Mast Camera Zoom (Mastcam-Z) Multispectral, Stereoscopic Imaging Investigation. *Space Science Reviews*, *217*(1), 24. https://doi.org/10.1007/s11214-020-00755-x

Bell, J. F., & Maki, J. N. (2021). *Mars 2020 Mast Camera Zoom Data Bundle, from Operations Team, calibrated products*. Planetary Data System. https://doi.org/10.17189/BS6B-4782

Benison, K. C. (2017). Gypsum gravel devils in Chile: Movement of largest natural grains by wind? *Geology*, *45*(5), 423–426. https://doi.org/10.1130/g38901.1

Benison, K. C. (2019). The physical and chemical sedimentology of two high-altitude acid salars in Chile: Sedimentary processes in an extreme environment. *Journal of Sedimentary Research*, *89*(2), 147–167. https://doi.org/10.2110/jsr.2019.9

Benison, K. C., Bowen, B. B., Oboh-Ikuenobe, F. E., Jagniecki, E. A., LaClair, D. A., Story, S. L., et al. (2007). Sedimentology of acid saline lake in southern Western Australia: Newly-described processes and products of an extreme environment. *Journal of Sedimentary Research*, *77*(5), 366–388. https://doi.org/10.2110/jsr.2007.038

Berger, J. A., Schmidt, M. E., Gellert, R., Campbell, J. L., King, P. L., Flemming, R. L., et al. (2016). A global Mars dust composition refined by the Alpha-Particle X-ray Spectrometer in Gale Crater. *Geophysical Research Letters*, *43*(1), 67–75. https://doi.org/10.1002/2015gl066675

Bishop, J. L. (2019). Chapter 4: Visible and near-infrared reflectance spectroscopy of geologic materials. In J. L. Bishop, J. F. BellIII, & J. E. Moersch (Eds.), *Remote compositional analysis: Techniques for understanding spectroscopy, mineralogy, and geochemistry of planetary surfaces*. Cambridge University Press.

Blake, D. F., Morris, R. V., Kocurek, G., Morrison, S. M., Downs, R. T., Bish, D., et al. (2013). Curiosity at Gale crater, Mars: Characterization and analysis of Rocknest sand shadow. *Science*, *341*(6153), 1239505. https://doi.org/10.1126/science.1239505

Brown, A. J., Viviano, C. E., & Goudge, T. A. (2020). Olivine-carbonate Mineralogy of the Jezero crater region. *Journal of Geophysical Research: Planets*, *125*(3), e2019JE006011. https://doi.org/10.1029/2019JE006011

Brückner, J., Dreibus, G., Rieder, R., & Waänke, H. (2003). Refined data of Alpha Proton X-ray Spectrometer analyses of soils and rocks at the Mars Pathfinder site: Implications for surface chemistry. *Journal of Geophysical Research*, *108*(E12), 8094. https://doi.org/10.1029/2003JE002060

Carrier, B. L., & Kounaves, S. P. (2015). The origins of perchlorate in the Martian soil. *Geophysical Research Letters*, *42*(10), 3739–3745. https://doi.org/10.1002/2015GL064290

Catling, D. C., Claire, M. W., Zahnle, K. J., Quinn, R. C., Clark, B. C., Hecht, M. H., & Kounaves, S. (2010). Atmospheric origins of perchlorate on Mars and in the Atacama. *Journal of Geophysical Research*, *115*, E00E11. https://doi.org/10.1029/2009JE003425

Chide, B., Beyssac, O., Gauthier, M., Benzerara, K., Esteve, I., Boulliard, J. C., et al. (2021). Acoustic monitoring of laser-induced phase transitions in minerals: Implication for Mars exploration with SuperCam. *Scientific Reports*, *11*(1), 24019. https://doi.org/10.1038/s41598-021-03315-7

Chide, B., Maurice, S., Cousin, A., Bousquet, B., Mimoun, D., Beyssac, O., et al. (2020). Recording laser-induced sparks on Mars with the SuperCam microphone. *Spectrochimica Acta Part B: Atomic Spectroscopy*, *174*, 106000. https://doi.org/10.1016/j.sab.2020.106000

Chou, I.-M., & Seal II, R. R. (2007). Magnesium and calcium sulfate stabilities and the water budget of Mars. *Journal of Geophysical Research*, *112*(E11), E11004. https://doi.org/10.1029/2007JE002898

Clark, B. C., Baird, A. K., Weldon, R. J., Tsusaki, D. M., Schnabel, L., & Candelariam, P. (1982). Chemical composition of Martian fines. *Journal of Geophysical Research*, *87*(B12), 10059–10067. https://doi.org/10.1029/jb087ib12p10059

Cloutis, E., Applin, D., Connell, S., Kubanek, K., Kuik, J., Parkinson, A., et al. (2021). A simulated rover exploration of a long-lived hypersaline spring environment: The East German Creek (MB, Canada) Mars analogue site. *Planetary and Space Science*, *195*, 105130. https://doi.org/10.1016/j.pss.2020.105130

Cousin, A., Meslin, P. Y., Wiens, R. C., Rapin, W., Mangold, N., Fabre, C., et al. (2015). Compositions of coarse and fine particles in Martian soils at Gale: A window into the production of soils. *Icarus*, *249*, 22–42. https://doi.org/10.1016/j.icarus.2014.04.052

David, G., Dehouck, E., Meslin, P.-Y., Rapin, W., Cousin, A., Forni, O., et al. (2022). Evidence for amorphous sulfates as the main carrier of soil hydration in Gale crater, Mars. *Geophysical Research Letters*, *49*(21), e2022GL098755. https://doi.org/10.1029/2022GL098755

Edwards, H. G. M., Villar, S. E. J., Parnell, J., Cockell, C. S., & Lee, P. (2005). Raman spectroscopic analysis of cyanobacterial gypsum halotrophs and relevance for sulfate deposits on Mars. *Analyst*, *130*(6), 917–923. https://doi.org/10.1039/B503533C

Ehlmann, B. L., Edgett, K. S., Sutter, B., Achilles, C. N., Litvak, M. L., Lapotre, M. G. A., et al. (2017). Chemistry, mineralogy, and grain properties at Namib and high dunes, Bagnold dune field, Gale crater, Mars: A synthesis of Curiosity rover observations. *Journal of Geophysical Research: Planets*, *122*(12), 2510–2543. https://doi.org/10.1002/2017JE005267

Ericksen, G. E. (1981). Geology and origin of the Chilean nitrate deposits. https://doi.org/10.3133/pp1188

Fischer, E., Martínez, G. M., Rennó, N. O., Tamppari, L. K., & Zent, A. P. (2019). Relative humidity on Mars: New results from the Phoenix TECP sensor. *Journal of Geophysical Research: Planets*, *124*(11), 2780–2792. https://doi.org/10.1029/2019je006080

Fishbaugh, K. E., Poulet, F., Chevrier, V., Langevin, Y., & Bibring, J.-P. (2007). On the origin of gypsum in the Mars north polar region. *Journal of Geophysical Research*, *112*(E7), E07002. https://doi.org/10.1029/2006JE002862

Forni, O., Maurice, S., Gasnault, O., Wiens, R. C., Cousin, A., Clegg, S. M., et al. (2013). Independent component analysis classification of laser induced breakdown spectroscopy spectra. *Spectrochimica Acta Part B: Atomic Spectroscopy*, *86*, 31–41. https://doi.org/10.1016/j.sab.2013.05.003

Fouchet, T., Reess, J. M., Montmessin, F., Hassen-Khodja, R., Nguyen-Tuong, N., Humeau, O., et al. (2022). The SuperCam infrared spectrometer for the perseverance rover of the Mars2020 mission. *Icarus*, *373*, 114773. https://doi.org/10.1016/j.icarus.2021.114773

Gabriel, T. S. J., Hardgrove, C., Czarnecki, S., Rampe, E. B., Rapin, W., Achilles, C. N., et al. (2018). Water abundance of dunes in Gale crater, Mars from active neutron experiments and implications for amorphous phases. *Geophysical Research Letters*, *45*(23), 12–766. https://doi.org/10.1029/2018gl079045

Garczynski, B. J., Bell, J. F., III, Horgan, B. H. N., Johnson, J. R., Rice, M. S., Vaughan, A., et al. (2022). Perseverance and the purple coating: A Mastcam-Z story. In *Lunar and Planetary Science Conference* (Vol. 53).

Gasnault, O., Virmontois, C., Maurice, S., Wiens, R. C., Le Mouélic, S., Bernardi, P., et al. (2021). What SuperCam will see: The Remote Micro-Imager aboard Perseverance. In *Lunar and Planetary Science Conference*. Abstract #2248.

Hanley, J., Chevrier, V. F., Berget, D. J., & Adams, R. D. (2012). Chlorate salts and solutions on Mars. *Geophysical Research Letters*, *39*(8), L08201. https://doi.org/10.1029/2012gl051239

Hayes, A. G., Corlies, P., Tate, C., Bell III, J. F., Maki, J. N., Caplinger, M., et al. (2021). Pre-flight calibration of the Mars 2020 Rover Mastcam Zoom (Mastcam-Z) multispectral, stereoscopic imager. *Space Science Reviews*, *217*(2), 29. https://doi.org/10.1007/s11214-021-00795-x

Hecht, M. H., Kounaves, S. P., Quinn, R. C., West, S. J., Young, S. M. M., Ming, D. W., et al. (2009). Detection of perchlorate and the soluble chemistry of Martian soil at the Phoenix landing site. *Science*, *325*(5936), 64–67. https://doi.org/10.1126/science.1172466

Hughes, K. A., & Lawley, B. (2003). A novel Antarctic microbial endolithic community within gypsum crusts. *Environmental Microbiology*, *5*(7), 555–565. https://doi.org/10.1046/j.1462-2920.2003.00439.x

iMOST. (2018). In D. W. Beaty, M. M. Grady, H. Y. McSween, E. Sefton-Nash, B. L. Carrier, F. Altieri, et al. (Eds.), *The Potential Science and Engineering Value of Samples Delivered to Earth by Mars Sample Return* (p. 186). MEPAG. Retrieved from https://mepag.jpl.nasa.gov/reports.cfm

Kinch, K. M., Madsen, M. B., Bell, J. F., III, Maki, J. N., Bailey, Z., Hayes, A. G., et al. (2020). Radiometric calibration targets for the Mastcam-Z Camera on the Mars 2020 Rover mission. *Space Science Reviews*, *216*(8), 141. https://doi.org/10.1007/s11214-020-00774-8

Kounaves, S. P., Chaniotakis, N. A., Chevrier, V. F., Carrier, B. L., Folds, K. E., Hansen, V. M., et al. (2014). Identification of the perchlorate parent salts at the Phoenix Mars landing site and possible implications. *Icarus*, *232*, 226–231. https://doi.org/10.1016/j.icarus.2014.01.016

Kounaves, S. P., Hecht, M. H., Kapit, J., Quinn, R. C., Catling, D. C., Clark, B. C., et al. (2010). Soluble sulfate in the Martian soil at the Phoenix landing site. *Geophysical Research Letters*, *37*(9), L09201. https://doi.org/10.1029/2010GL042613

Lasue, J., Cousin, A., Meslin, P. Y., Mangold, N., Wiens, R. C., Berger, G., et al. (2018). Martian eolian dust probed by ChemCam. *Geophysical Research Letters*, *45*(20), 10968–10977. https://doi.org/10.1029/2018gl079210

Liu, Y., Tice, M. M., Schmidt, M. E., Treiman, A. H., Kizovski, T. V., Hurowitz, J. A., et al. (2022). An olivine cumulate outcrop on the floor of Jezero crater. *Mars*, *377*(6614), 1513–1519. https://doi.org/10.1126/science.abo2756

Lybrand, R. A., Bockheim, J. G., Ge, W., Graham, R. C., Hlohowskyj, S. R., Michalski, G., et al. (2016). Nitrate, perchlorate, and iodate co-occur in coastal and inland deserts on Earth. *Chemical Geology*, *442*, 174–186. https://doi.org/10.1016/j.chemgeo.2016.05.023

Maki, J. N., Deen, R. G., Algermissen, S., Dunn, A. E., Toole, N. T., Crombie, M. K., et al. (2020a). Raw data products for the Mars 2020 Perseverance Rover Hazard Cameras. https://doi.org/10.17189/282b-1524

Maki, J. N., Deen, R. G., Algermissen, S., Dunn, A. E., Toole, N. T., Crombie, M. K., et al. (2020b). Raw data products for the Mars 2020 Perseverance Rover Navigation Cameras. https://doi.org/10.17189/d3nm-pp09

Mandon, L., Quantin-Nataf, C., Royer, C., Beck, P., Fouchet, T., Johnson, J. R., et al. (2023). Reflectance of Jezero crater floor: 2. Mineralogical interpretation. *Journal of Geophysical Research: Planets*, *128*, e2022JE007450. https://doi.org/10.1029/2022JE007450

Marchant, D. R., & Head, J. W. (2007). Antarctic dry valleys: Microclimate zonation, variable geomorphic processes, and implications for assessing climate change on Mars. *Icarus*, *192*(1), 187–222. https://doi.org/10.1016/j.icarus.2007.06.018

Martínez, G. M., Fischer, E., Rennó, N. O., Sebastián, E., Kemppinen, O., Bridges, N., et al. (2016). Likely frost events at Gale crater: Analysis from MSL/REMS measurements. *Icarus*, *280*, 93–102. https://doi.org/10.1016/j.icarus.2015.12.004

Martínez, G. M., Sebastián, E., Vicente-Retortillo, A., Smith, M. D., Johnson, J. R., Fischer, E., et al. (2023). Surface energy budget, albedo and thermal inertia at Jezero Crater, Mars, as observed from the Mars 2020 MEDA instrument. *Journal of Geophysical Research: Planets*, *128*(2), e2022JE007537. https://doi.org/10.1029/2022JE007537

Maurice, S., Chide, B., Murdoch, N., Lorenz, R. D., Mimoun, D., Wiens, R. C., et al. (2022). In situ recording of Mars soundscape. *Nature*, *605*, 652–658. https://doi.org/10.1038/s41586-022-45904679-0

Maurice, S., Wiens, R. C., Bernardi, P., Caïs, P., Robinson, S., Nelson, T., et al. (2021). The SuperCam instrument suite on the Mars 2020 Rover: Science objectives and mast-unit description. *Space Science Reviews*, *217*(3), 47. https://doi.org/10.1007/s11214-021-00807-w

Meslin, P. Y., Forni, O., Beck, P., Cousin, A., Beyssac, O., Lopez-Reyes, G., et al. (2023). Evidence for late perchlorate and sulfate salts deposition in Jezero crater, Mars, from SuperCam observations. In *Lunar and Planetary Science Conference* (Vol. 53, p. 2694).

Meslin, P.-Y., Gasnault, O., Forni, O., Schroder, S., Cousin, A., Berger, G., et al. (2013). Soil diversity and hydration as observed by ChemCam at Gale Crater, Mars. *Science*, *341*(6153), 1238670. https://doi.org/10.1126/science.1238670

Michalski, G., Scott, Z., Kabiling, M., & Thiemens, M. H. (2003). First measurements and modeling of $\Delta^{17}O$ in atmospheric nitrate. *Geophysical Research Letters*, *30*(16), 1870. https://doi.org/10.1029/2003GL017015

Moeller, R. C., Jandura, L., Rosette, K., Robinson, M., Samuels, J., Silverman, M., et al. (2021). The Sampling and Caching Subsystem (SCS) for the scientific exploration of Jezero crater by the Mars 2020 Perseverance rover. *Space Science Reviews*, *217*, 5. https://doi.org/10.1007/s11214-020-00777-5

Moore, H. J., Hutton, R. E., Clow, G. D., & Spitzer, C. R. (1987). Physical properties of the surface materials at the Viking landing sites on Mars. *United States Geological Survey Professional Paper 1389*. Retrieved from https://pubs.usgs.gov/pp/1389/report.pdf

Mustard, J. F., Adler, M., Allwood, A., Bass, D. S., Beaty, D. W., Bell, J. F., III, et al. (2013). *Report of the Mars 2020 Science Definition Team* (p. 154). Mars Exploration Program Analysis Group (MEPAG). Retrieved from http://mepag.jpl.nasa.gov/reports/MEP/Mars_2020_SDT_Report_Final.pdf

Paar, G., Ortner, T., Tate, C., Deen, R. G., Abercrombie, P., Vona, M., et al. (2023). Three-dimensional data preparation and immersive mission-spanning visualization and analysis of Mars 2020 Mastcam-Z stereo image sequences. https://doi.org/10.1029/2022EA002532

Pieters, C. M., & Hiroi, T. (2004). RELAB (Reflectance Experiment Laboratory): A NASA Multiuser Spectroscopy Facility.

Polkko, J., Hieta, M., Harri, A. M., Tamppari, L., Martínez, G., Viúdez-Moreiras, D., et al. (2023). Initial results of the relative humidity observations by MEDA instrument onboard the Mars 2020 Perseverance rover. *Journal of Geophysical Research: Planets*, *128*(2). (this issue). https://doi.org/10.1029/2022je007447

Ramachandran, A. V., Zorzano, M.-P., & Martín-Torres, J. (2021). Experimental Investigation of the atmosphere-Regolith water Cycle on present-day Mars. *Sensors*, *21*(21), 7421. https://doi.org/10.3390/s21217421

Rampe, E. B., Bristow, T. F., Morris, R. V., Morrison, S. M., Achilles, C. N., Ming, D. W., et al. (2020). Mineralogy of Vera Rubin ridge from the Mars Science Laboratory CheMin instrument. *Journal of Geophysical Research: Planets*, *125*(9), e2019JE006306. https://doi.org/10.1029/2019JE006306

Rampe, E. B., Morris, R. V., Archer, P. D., Agresti, D. G., & Ming, D. W. (2016). Recognizing sulfate and phosphate complexes chemisorbed onto nanophase weathering products on Mars using in-situ and remote observations. *American Mineralogist*, *101*(3), 678–689. https://doi.org/10.2138/am-2016-5408CCBYNCND

Rivera-Valentín, E., Martínez, G., Filiberto, J., Lynch, K., Chevrier, V. F., Gough, R. V., et al. (2020). Resolving the water cycle on a salty Mars: Planetary science and astrobiology exploration strategies for the next decade. *Bulletin of the American Astronomical Society*, *53*(4). https://doi.org/10.3847/25c2cfeb.b0e3963b

Rodriguez-Manfredi, J. A., & de la Torre Juarez, M. (2021). *Mars 2020 Perseverance Rover Mars Environmental Dynamics Analyzer (MEDA) Experiment Data Record (EDR) and Reduced Data Record (RDR) data products archive bundle*. PDS Atmospheres Node. https://doi.org/10.17189/1522849

Rodriguez-Manfredi, J. A., De la Torre Juárez, M., Alonso, A., Apéstigue, V., Arruego, I., Atienza, T., et al. (2021). The Mars Environmental Dynamics Analyzer, MEDA. A Suite of Environmental Sensors for the Mars 2020 Mission. *Space Science Reviews*, *217*(3), 48. https://doi.org/10.1007/s11214-021-00816-9

Royer, C., Fouchet, T., Mandon, L., Montmessin, F., Poulet, F., Forni, O., et al. (2023). Reflectance of Jezero crater floor: 1. Data processing and calibration of the infrared spectrometer (IRS) on SuperCam. *Journal of Geophysical Research: Planets*, *128*(1), e2022JE007481. https://doi.org/10.1029/2022je007481

Scheller, E. L., Hollis, J. R., Cardarelli, E. L., Steele, A., Beegle, L., Bhartia, R., et al. (2022). Aqueous alteration processes in Jezero crater, Mars—Implications for organic geochemistry. *Science*, *378*(6624), 1105–1110. https://doi.org/10.1126/science.abo5204

Schmidt, M. E., Perrett, G. M., Bray, S. L., Bradley, N. J., Lee, R. E., Berger, J. A., et al. (2018). Dusty rocks in Gale crater: Assessing areal coverage and separating dust and rock contributions in APXS analyses. *Journal of Geophysical Research: Planets*, *123*(7), 1649–1673. https://doi.org/10.1029/2018je005553

Sebastián, E., Martínez, G., Ramos, M., Pérez-Grande, I., Sobrado, J., & Manfredi, J. A. R. (2021). Thermal calibration of the MEDA-TIRS radiometer onboard NASA's Perseverance rover. *Acta Astronautica*, *182*, 144–159. https://doi.org/10.1016/j.actaastro.2021.02.006

Sharma, S., Roppel, R. D., Murphy, A., Beegle, L. W., Bhartia, R., Steele, A., et al. (2022). *Mapping organic-mineral associations in the Jezero crater floor*. American Geophysical Union.

Singer, M. J., & Shainberg, I. (2004). Mineral soil surface crusts and wind and water erosion. *Earth Surface Processes and Landforms*, *29*(9), 1065–1075. https://doi.org/10.1002/esp.1102

Skelley, A. M., Scherer, J. R., Aubrey, A. D., Grover, W. H., Ivester, R. H. C., Ehrenfreund, P., et al. (2005). Development and evaluation of a microdevice for amino acid biomarker detection and analysis on Mars. *Proceedings of the National Academy of Sciences*, *102*(4), 1041–1046. https://doi.org/10.1073/pnas.0406798102

Smoot, J. P., & Castens-Seidell, B. (1994). Sedimentary features produced by efflorescent salt crusts, Saline Valley and Death Valley, California. In R. Renaut & W. M. Last (Eds.), *Sedimentology and Geochemistry of Modern and Ancient Lakes* (Vol. 50, pp. 73–90). SEPM Special Publication.

Stern, J. C., Sutter, B., Freissinet, C., Navarro-González, R., McKay, C. P., Archer, P. D., Jr., et al. (2015). Evidence for indigenous nitrogen in sedimentary and aeolian deposits from the Curiosity rover investigations at Gale crater, Mars. *Proceedings of the National Academy of Sciences*, *112*(14), 4245–4250. https://doi.org/10.1073/pnas.1420932112

Sullivan, R., Anderson, R., Biesiadecki, J., Bond, T., & Stewart, H. (2011). Cohesions, friction angles, and other physical properties of Martian regolith from Mars Exploration Rover wheel trenches and wheel scuffs. *Journal of Geophysical Research*, *116*(E2), E02006. https://doi.org/10.1029/2010JE003625

Sun, V. Z., Hand, K. P., Stack, K. M., Farley, K. A., Simon, J. I., Newman, C., et al. (2023). Overview and results from the Mars 2020 Perseverance rover's first science campaign on the Jezero crater floor. *Journal of Geophysical Research: Planets*, *128*, e2022JE007613. https://doi.org/10.1029/2022JE007613

Tan, J., Lewis, J. M. T., & Sephton, M. A. (2018). The fate of lipid biosignatures in a Mars-analogue sulfur stream. *Scientific Report*, *8*(1), 7586. https://doi.org/10.1038/s41598-018-25752-7

Tice, M. M., Hurowitz, J. A., Allwood, A. C., Jones, M. W. M., Orenstein, B. J., Davidoff, S., et al. (2022). Alteration history of Seitah formation rocks inferred by PIXL X-ray fluorescence, X-diffraction, and multispectral imaging on Mars. *Science Advances*, *8*(47). https://doi.org/10.1126/sciadv.abp9084

Turenne, N., Sidhu, S., Applin, D., & Cloutis, E. (2022). Nontronite spectral reflectance characteristics with implications for Mars. In *Lunar and Planetary Science Conference* (Vol. 53). abstract #1571.

Vaughan, A., Minitti, M. E., Cardarelli, E. L., Johnson, J. R., Kah, L. C., Pilleri, P., et al. (2023). Regolith of the crater floor units, Jezero crater, Mars: Textures, composition and implications for provenance. *Journal of Geophysical Research: Planets*, *128*, e2022JE007437. https://doi.org/10.1029/2022JE007437

Wang, A., Bell, J. F., III, Li, R., Johnson, J. R., Farrand, W. H., Cloutis, E. A., et al. (2008). Light-toned salty soils and coexisting Si-rich species discovered by the Mars Exploration Rover Spirit in Columbia Hills. *Journal of Geophysical Research*, *113*(E12), E12S40. https://doi.org/10.1029/2008JE003126

Wiens, R. C., Maurice, S., Robinson, S. H., Nelson, A. E., Cais, P., Bernardi, P., et al. (2021). The SuperCam instrument suite on the NASA Mars 2020 rover: Body unit and combined system tests. *Space Science Reviews*, *217*(1), 4. https://doi.org/10.1007/s11214-020-00777-5

Wiens, R. C., Maurice, S. A., Deen, R. G., Padgett, D., Algermissen, S., Dunn, A. E., et al. (2021). Mars 2020 Perseverance rover SuperCam raw, calibrated, and derived data products. https://doi.org/10.17189/1522646

Wierzchos, J., Camara, B., De los Rios, A., Davila, A. F., Sanchez Almazo, I. M., Artieda, O., et al. (2011). Microbial colonization of Ca-sulfate crusts in the hyperarid core of the Atacama Desert: Implications for the search for life on Mars. *Geobiology*, *9*(1), 44–60. https://doi.org/10.1111/j.1472-4669.2010.00254.x

Yang, L., Xing, W., Sara, Z. Y.-Y., Lu, P., Chi, W., Jia, L., et al. (2022). Zhurong reveals recent aqueous activities in Utopia Planitia, Mars. *Science Advances*, *8*(19), eabn8555. https://doi.org/10.1126/sciadv.abn8555

Yen, A. S., Gellert, R., Schröder, C., Morris, R. V., Bell, J. F., Knudson, A. T., et al. (2005). An integrated view of the chemistry and mineralogy of Martian soils. *Nature*, *436*(7047), 49–54. https://doi.org/10.1038/nature03637